USGS Award No. G15AP00024
Award Period: 01/01/2015 – 12/31/2016

CHARACTERIZING THE IMPACT OF SOURCE TYPE, OFFSET, AND RECEIVER SPACING ON EXPERIMENTAL MASW DATA USING LOVE WAVES

Joseph T. Coe[1], Siavash Mahvelati[1], and Jonathan E. Nyquist[2]

[1] Department of Civil & Environmental Engineering, Temple University, Philadelphia, PA
[2] Department of Earth & Environmental Science, Temple University, Philadelphia, PA

Principal Investigators:

Joseph Thomas Coe, Jr., Ph.D.
Department of Civil & Environmental Engineering
Temple University, 1947 North 12th Street, ENGR Building Room 518
Philadelphia, PA 19122-6018
Office: (215)204-6100, Fax: (215)204-4696, joseph.coe@temple.edu

Jonathan E. Nyquist
Department of Earth & Environmental Science
Temple University, 1901 North 13th Street, Beury Hall Room 319
Philadelphia, PA 19122-6018
Office: (215)204-7484, Fax: (215)204-3496, nyq@temple.edu

Graduate Student Researcher:

Siavash Mahvelati
Department of Civil & Environmental Engineering
Temple University, 1947 North 12th Street, ENGR Building Room 518
Philadelphia, PA 19122-6018
smahvelati@temple.edu

Final Technical Report

May 4, 2018

TABLE OF CONTENTS

LIST OF FIGURES

LIST OF TABLES

ABSTRACT

The Multichannel Analysis of Surface Wave (MASW) method is increasingly utilized in subsurface investigations for seismic design purposes in research and practice. Much of the development of MASW has focused on Rayleigh waves (i.e., MAS_RW), which are generated from vertical impacts at the ground surface. There has been comparably less research regarding the use of Love waves in MASW (i.e., MAS_LW) as generated from horizontal impacts despite potential benefits related to inversion uniqueness and accuracy. In fact, information regarding optimal MAS_LW field data acquisition is generally unavailable or not quantified on the basis of experimental studies. In this study, three test sites in the southeastern Pennsylvania area were investigated using both MAS_RW and MAS_LW. The field sites represented a range of conditions commonly encountered in the field, including a thin low velocity layer overlying stiff bedrock, a thicker low velocity layer overlying stiff bedrock, and a more subtle transition in velocity between soils and underlying bedrock. Collocation of the MAS_RW and MAS_LW receiver arrays allowed a direct comparison between data acquired from the two approaches with respect to each other and "ground truth" models inferred from seismic refraction and downhole testing. Multiple source types, source offsets, and receiver spacings were utilized to examine their impacts on data quality and interpretation and any differences encountered between Rayleigh and Love wave testing. The results from this research program provide an experimental basis for recommendations regarding field survey parameters and Love wave source types as well as quantification of the improvement offered by Love wave surveys. The research findings indicated that minimum offset required to avoid near-field effects was slightly longer for Love waves relative to Rayleigh waves. Rayleigh wave dispersion curves were negatively affected by appreciable scatter when the source offset was varied. Love waves seemed immune to this effect. Love waves also more consistently excited the fundamental mode, while Rayleigh wave dispersion image were affected by the presence of higher mode energy. This made interpretation of the fundamental mode dispersion curves more difficult for Rayleigh waves and decreased confidence in their subsequent inversions. Consequently, the V_S profiles obtained in this study from Love waves generally agreed better with the ground truth models established based on seismic refraction and downhole testing. Love waves were also capable of resolving V_S to larger depths than Rayleigh waves due to higher phase velocity and correspondingly longer wavelengths.

1. INTRODUCTION

Seismic wave propagation highly depends on the properties of the propagating medium. Investigating seismic wave propagation can therefore reveal key information regarding the properties of earthen materials below the ground surface. For instance, the shear modulus of a soil (G) is a key parameter that generally defines its stiffness against shear strains. The importance of shear modulus has been widely recognized in liquefaction assessments, ground motion prediction, and ground response analysis. The shear modulus of geomaterials highly depends on strain level, but when measured at a small-strain level (10^{-3}% or less), it is directly related to the shear wave velocity (V_S) of the soil ($G_{max} = \rho V_s^2$). Shear wave velocity has long been known to be a valuable indicator of the dynamic properties of earthen materials and has been adopted widely to establish design response spectra and seismic site classifications.

Several laboratory and in-situ techniques have been developed to estimate VS of subsurface profiles. The most common approach is the use of seismic geophysical testing. Such methods utilize elastic wave propagation to identify changes in stiffness and density. In situ seismic geophysical methods can be categorized into invasive (i.e., disruptive to the site conditions) and non-invasive methods. Examples of invasive methods are downhole testing, P-S logging, and cross-hole testing. These methods are typically time intensive and require costly boreholes. Non-invasive seismic geophysical methods on the other hand, can address some of limitations of invasive methods. Methods such as seismic refraction and reflection acquire body wave information [primary (P-) and shear (S-) wave] while surface wave methods rely on measurements of surface waves (i.e., waves travelling along a very shallow part of a given medium) to estimate VS profiles. Although Rayleigh, Love, Scholte, and Stoneley are all different types of surface waves, Rayleigh and Love waves are the two types that are most commonly used in engineering applications.

1.1. Surface Wave Methods

Prior to the development of surface wave methods, surface waves (sometime referred to as *ground roll*) were usually considered as coherent "noise" masking useful body wave signals and efforts were made to diminish them from the field recordings. Still, the literature shows evidence of the use of surface waves dating back to the 1950s. The efforts by Van der Pol (1951) and Jones (1955, 1958) includes the use of steady-state vibration method which later was developed into the continuous surface-wave (CSW) method (Abbiss 1981). CSW is a two-channel technique in which one receiver is responsible for generating vibratory input source and is placed on the ground surface and is excited at a number of known frequencies. The other receiver, acting as a recorder of Rayleigh vibrations, is placed at different offsets from the source to locate peaks in surface displacement. This information was used to determine the phase lag between consecutive surface wave amplitude from which V_S could eventually be estimated. In the early

1980s, the Spectral Analysis of Surface Waves (SASW) method was introduced to address some of the limitation of CSW (Heisey et al. 1982, Nazarian and Stokoe 1984). SASW is a two- (or four-) receiver method that analyzes the phase spectra of surface waves generated from impact sources. SASW experienced significant advances in the coming years and became a popular tool in various engineering applications (e.g., Kim et al., 2001; Madhyannapu et al., 2009; Green et al. 2011). However, some limitations in the SASW method remained due to the smaller number of receivers used to acquire the surface wave signals. A number of these issues were addressed when a research team at the Kansas Geological Survey developed the Multichannel Analysis of Surface Waves (MASW) method to determine the stiffness of subsurface profiles (Park et al., 1999; Xia et al., 1999). Since the inception of MASW, many have used this method as a non-destructive geophysical and geotechnical tool for a variety of applications including seismic site classification (e.g., Kanlı et al. 2006; Anbazhagan and Sitharam 2010), void detection (e.g., Xia et al. 2004; 2007), assessment of ground improvement (e.g., Burke and Schofield 2008; Waddell et al. 2010), mapping bedrock/fault zone (e.g., Miller et al. 1999; Ivanov et al. 2006), and seismic zonation (e.g., Yilmaz et al. 2009). The large number of receivers (typically 24+ as in Figure 1) increases the robustness of MASW data acquisition and processing relative to its predecessor the SASW method.

1.1.1. Multichannel Analysis of Surface Waves (MASW)

Three basic elements are involved in a typical MASW survey: a series of geophones (typically, 24 or 48), a seismic source, and an acquisition system. Surface waves generated using a seismic source are collected by a series of receivers usually deployed as a linear array, and recorded waveforms are collected and digitized by the data acquisition system (Figure 1). A seismic source inputs energy into the subsurface by generating seismic waves. Sledgehammers, accelerated weight drops (AWD), shotguns, explosive chargers, and electromagnetic shakers are examples of commonly used sources in MASW surveys. However, among the mentioned sources, sledgehammers are among the common sources used in MASW surveys due to their cost-effectiveness and quick data collection. The frequency range of the generated surface wave is highly dependent on the source, but as a rule of thumb, the smaller the source, the higher the dominant frequency and vice versa meaning that "*heavier*" sources are capable of inputting wavelets with lower frequency ranges. The seismic signal produced by a specific source is affected by a number of parameters including seismic source characteristics, surface and subsurface conditions (Herbst et al. 1998; Yordkayhun et al. 2009). Multiple impacts are at a certain offset are recorded, and stacked (i.e., averaged) to reduce undesirable effects of random noise. As a rule of thumb, stacking N shots records increases the signal-to-noise ratio by a factor of $\sqrt{N}$ where N is the number of recorded impacts (Foti et al. 2015).

In addition to active data collection with a specific seismic source, surface wave measurements can be accomplished by adopting a passive approach. Passive measurements do not rely on using an active seismic source, and usually record much lower frequency (i.e., larger wavelengths) surface waves leading to larger depths of investigation. Some examples of the ambient noise sources are nearby traffic (Park and Miller 2008; Obando et al. 2009; Behm and Snieder 2013), trains (Motazedian et al. 2012; Nolan et al. 2013), artificial blasting (Ha et al. 2013), and ocean waves (Carnevale and Park 2010). Longer arrays of geophones as well as longer recording times are necessary to ensure that enough background noise with longer wavelengths are recorded. The target frequency range of a passive MASW survey is approximately in the range of 2-20 Hz (Park and Carnevale 2014).

Depending on the impact method, Rayleigh or Love waves can be generated. Rayleigh waves are constructed by the interference of compressional waves (P-waves) and vertically polarized shear wave (i.e., S_V-wave) energy. Particles motion in such waves is located on an elliptical path along a vertical plane that is consistent with the direction of wave propagation (Figure 2a). The amplitude of Rayleigh waves decreases exponentially with depth. Rayleigh wave propagation depends on wave frequency, *Vs*, P-wave velocity (V_P), thickness of the subsurface layers, and soil density (Xia et al. 1999). Love waves, mathematically introduced by A.E.H. Love in 1911, only contain horizontally polarized shear wave (i.e., S_H-wave) energy (Love 1911). Particle motion in Love waves is parallel to the ground surface and perpendicular to the direction of wave propagation (Figure 2b). In contrast to Rayleigh waves, Love wave propagation is not a function of V_P and is only characterized by V_S, thickness of the subsurface layers, and material density. Love waves are prevalent in situations where a layer with a higher stiffness underlies a low-velocity layer, and they cannot be generated in homogeneous half-space media (Foti et al. 2015). Similar to Rayleigh waves, Love wave amplitude decays exponentially with depth.

In its simplest form, Rayleigh waves can be generated by vertical impacts from a sledgehammer (or an AWD). Typically, a base plate is used as a means to couple the impact source and increase the amount of energy introduced into the ground. In order to produce Love waves properly, the impact mechanism should be located perpendicular (or close to perpendicular) with respect to the ground surface, and good coupling must be provided between the coupler (base plate) and the ground surface to ensure that it does not move along the surface after each impact. The coupling between the horizontal source and ground surface is often reinforced by weighing down the base plate and/or by attaching spikes to the underside of the base plate. Due to the nature of Love waves, their generation necessitates the use of more sophisticated impact couplers than those used to generate Rayleigh waves. This could be a reason that explains why Love waves are less employed than Rayleigh waves in active seismic studies.

As surface waves propagate, they undergo what is referred to as dispersion. Love waves are inherently dispersive, whereas Rayleigh waves exhibit dispersion in non-uniform (i.e. increasing stiffness) soil profiles. Dispersion refers to the fact that different frequency components of the input surface wave travel at different phase velocities. This occurs because the depth of penetration of a surface wave is proportional to its wavelength (λ). A broadband surface wave (i.e., a range of frequency components in the signal) will therefore "sample" different depths of the subsurface based on the corresponding wavelengths present in the signal. The phase velocity of each wavelength (or frequency) component will depend on the mechanical properties of the sampled layers involved in the wave propagation. A characteristic dispersion curve can be extracted for a site that represents the frequency (or wavelength) dependency of the phase velocity based on the underlying subsurface stratigraphy. This dispersion curve can be quite complex and difficult to interpret, particularly in situations where higher modes are present in the data. More than one phase velocity can be associated with a given frequency. Similar in concept to the vibration of a system of multi-degree of freedom, soil profiles can experience different modes of displacement. In such cases, the slowest phase velocity is related to the fundamental mode and the rest belong to higher modes. In a profile with gradually increasing V_S, the fundamental mode will be dominant (Foti et al. 2015). However, higher modes can play a major role when a stiff top layer (e.g., pavement layer) is underlain by layers of softer materials or when there is an abrupt change in the stiffness (e.g., shallow bedrock underneath a soft top layer) (Foti et al. 2015).

Another aspect of dispersion is the concept of higher modes. Similar in concept to the vibration of a system of multi-degree of freedom, soil profiles can experience different modes of vibration. Solving a surface wave dispersion equation (Rayleigh or Love) yields different number of nodal planes which are points of no particle displacement. The most basic mode of particle displacement is called the fundamental mode and more complex ones are referred to as higher modes. Figure 3 is an example showing four modes of Rayleigh wave displacement for a layered medium. In the presence of higher modes, more than one phase velocity can be associated with a given frequency. In such cases, the slowest phase velocity is related to the fundamental mode and the rest belong to higher modes. Higher modes can only exist above their cut-off frequency that is the lower frequency limit above which that specific mode can mathematically appear. In a profile with gradually increasing shear wave velocities, the fundamental mode will be dominant (Foti et al. 2015). However, higher modes can play a major role in two scenarios: (1) higher modes are likely to appear at higher frequencies when a stiff top layer (e.g., pavement layer) is underlain by layers of softer materials; and (2) higher modes can exist at lower frequency ranges in the presence of an abrupt change in the stiffness (e.g., shallow bedrock underneath a soft top layer) (Foti et al. 2015).

Development of the dispersion curve in MASW proceeds by generating an image space that represents wave energy accumulation, typically in the frequency-phase velocity domain (f-C_f). This dispersion image is often referred to as an overtone image. The multichannel record in time-space (t-x) domain is transformed into this domain using a number of spectral transformation methods: frequency-wavenumber (f-k) spectrum, slowness-frequency (p-w) transformation (McMechan and Yedlin 1981), and phase-shift method (Park et al. 1998). However, it has been shown that the quality of dispersion images generated by the phase-shift method is typically superior to those obtained by other methods (Park et al. 1998). The phase-shift method is implemented in many commercially developed geophysical software packages designed for surface-wave analysis including the Geometrics SeisImager/SW software used in the current study. The phase-shift method initially proceeds by applying a Fourier transform to the time domain to transform offset-time raw data into an offset-frequency domain. This offset-frequency domain is a combined function of amplitude and phase spectra in which amplitude contains properties of attenuation, spherical divergence, and related information, and the phase spectra part represents phase velocity-frequency relation. In the next step, for each offset at given phase velocities and frequencies, the phase shift required to counterbalance the time delay associated with that specific offset is determined and applied. Then, at certain frequency intervals (e.g., 1 Hz intervals), transformed traces are added using an integral function. Examining each frequency will reveal at least one phase velocity that provides the maximum value of accumulated energy for the integral. This point is picked as the phase velocity at that given frequency. Higher modes may appear if the energy is maximized at more than one point at a specific frequency. Trends in energy accumulation are then used in the transformed domain to extract dispersion curves.

Once the dispersion curve has been developed, the corresponding V_S profile can then be obtained by matching the experimental dispersion curve to a theoretical dispersion curve from forward modeling with an idealized subsurface model. Solving this inversion problem is an iterative process that is inherently nonlinear, ill-posed, and mixed-determined (Cox and Teague, 2016). Recommendations suggest that the initial velocity model be estimated as a percentage of the phase velocity (usually 110%) and assigned to a depth of 1/3-1/2 of the wavelength (Stokoe et al. 1994). Common inversion methods (e.g., methods by Forbriger 2003 a,b; O'Neill 2003; Bohlen et. al 2004) are based on linear algorithms in which V_S is the only parameter that is updated after each iteration, and other parameters such as the layer thickness, density, and Poisson ratio (in case of Rayleigh wave inversion) are kept as the original values assigned by the user. Optimization is necessary to ensure the most probable solution is obtained [e.g. least-squares method (deterministic)], though there are always concerns with non-uniqueness of the final solution. The use of additional information can help constrain the inversion process and ensure the final solution is appropriate for the site.

Surface wave methods offer a number of advantages over the conventional invasive and non-invasive seismic techniques. Typically, MASW results are easier to interpret than those from refraction/reflection methods in which first arrival determination could be challenging and subjected to users' interpretation (Foti et al. 2015). MASW is also capable of resolving stiff-over-soft velocity profiles, something that is impossible with the seismic refraction technique. Surface waves generally have higher signal-to-noise ratio due to their high-energy nature relative to body waves (Foti et al. 2015). When specifically compared to P-waves, surface waves are less affected by fluid saturation, and can provide shorter wavelength components with better resolution (Dasois et al. 1999). Moreover, due to their cylindrical wavefront, the geometrical attenuation of surface waves is lower than the attenuation of body waves which have spherical wavefronts (Stokoe and Santamarina 2000).

As with any testing methodology, MASW does suffer from some inherent limitations. For example, the minimum frequency of produced surface waveforms is limited and therefore poses a limit on the maximum depth of investigation (Tokimatsu 1997). Second, the quality of signals can be affected by near-field and far-field effects. Basically, a minimum distance from the seismic source is required for the surface waves to be properly developed (near-field effect). On the other hand, at greater distances from the source, surface waves are attenuated and background noise will be the dominant components instead of surface waves (far-field effect). Ongoing research is being conducted to comprehensively establish guidelines to avoid such artifacts. As previously highlighted, the inversion process used to estimate V_S from surface wave dispersion measurements is inherently non-unique, which means that multiple V_S profiles can have identical dispersion images. With regards to topography, V_S profiles estimated using MASW should be treated with caution for slopes greater than 10^o (Zeng et al. 2012). Most inversion algorithms assume that all subsurface layers are homogenous and flat across the area of interest (Foti et al. 2015). This can lead to erroneous results in sites with appreciable lateral heterogeneity. Finally, MASW resolution suffers as the depth of investigation increases since estimates of V_S are based on increasingly larger wavelengths that spatially average across more layers. This signifies that smaller lenses of soil may go unnoticed by MASW if they are located at significant depths in the profile.

1.1.2 MASW Using Love Waves

Rayleigh waves have generally received the most attention in the literature while Love waves are generally less employed in MASW. However, in the past few years, there has been a rise in the use of Love waves for site characterization purposes. MASW studies dealing with Love waves can be categorized into three general categories. The first category consists of studies focusing solely on the use of Love waves. Common tools used in this group of studies are analytical approaches (e.g., Guzina and Madyarov 2005), synthetic models and computer simulations (Luo et al. 2010; Hamimu et al. 2011), and field surveys (e.g., Winsborrow et al. 2003; Safani et al.

2006; Eslick et al. 2008; Xia et al. 2009). The second category is comprised of studies that made a comparison between Rayleigh and Love waves. Song et al. (1989) was among the first to systematically compare Rayleigh and Love waves. However, such studies have often been limited to a small number of collected field or synthesized seismic data. The third category of Love wave studies are focused on the joint analysis of seismic data where one set of input data is from Love wave testing (e.g., Misiek et al. 1997; Joh et al. 2006; Lane 2009; Dal Moro and Ferigo 2011; Boxberger et al. 2011).

The results from the aforementioned studies have led to a number of observations regarding Love waves in MASW testing. Song et al. (1989) examined target depths of Rayleigh and Love waves and concluded that at the same wavelength, Rayleigh wave penetrate deeper than Love waves. Love waves of longer wavelength are therefore necessary to reach the same target depth as that of Rayleigh waves. Yin et al. (2014) estimated that Rayleigh wave components sample 30-40% deeper than Love waves. Eslick et al. (2008) performed several Love wave surveys at a soft-over-bedrock site where the depth of the top soft layer was variable. They concluded that a 1 m of soft layer would be the minimum thickness required to recover promising seismic data in the frequency range of 5-50 Hz. It has been noted in several studies that Love wave dispersion images are often easier to interpret and less prone to mode misidentification (e.g., Lane 2009; Xia et al. 2010; Xia et. al. 2012; Yong et al. 2013). Due to their independence of V_P, Love wave inversion is also proven to be more stable and simpler compared to that from Rayleigh waves (e.g., Safani et al. 2005; Xia 2014). The resulting inverted profiles of Love waves can be more reliable due to a reduction in the issues related to non-uniqueness of the solution (Xia et al. 2012). Zeng et al. (2007) reported that Love waves are more sensitive to changes in V_S and thickness than Rayleigh waves over a wide frequency range. This means that Love waves can recover V_S profiles more accurately.

1.2 Motivation for This Study

The preceding discussion emphasizes that the mechanism of Love wave propagation is fundamentally different from that of Rayleigh waves. Much of our knowledge regarding optimal MASW field parameters have been formulated on the basis of Rayleigh waves (e.g., Park et al., 2002; Park and Carnevale, 2010). However, given the differences highlighted in multiple studies, there is some ambiguity as to whether optimal field parameters of MAS_RW can be applied confidently to MAS_LW. For instance, it was previously highlighted that at the same wavelength, Rayleigh waves can penetrate approximately 30-40% deeper into the subsurface than Love waves (Yin et al. 2014). Therefore, to achieve the same depth of investigation as Rayleigh wave testing, longer spread lengths would be necessary for Love wave surveys. Moreover, the majority of MAS_LW field experiments in the literature were conducted using a single impact source, limited source offsets, and receiver spacing. So much of the basic information regarding optimal field data acquisition parameters (e.g., source offsets, near/far-field effects, and receiver spacing)

is unavailable or not established based on experimental results. This study aims to fill this gap by exploring the effects of source type, offset, and receiver intervals on experimental MAS_LW data.

In the current study, three sites with different subsurface conditions in southeastern Pennsylvania were investigated using MASW testing with both Rayleigh and Love waves. Field efforts were performed using multiple source types, source offsets, and receiver spacings. Since all surveys were located in the same location at the sites, the results from this study allow a direct comparison of the effects of survey parameters on Rayleigh versus Love waves. In the following sections of the report, filed testing and data processing methods are discussed. This is followed by presentation of the results and discussion regarding the role of survey parameters on experimental MAS_RW and MAS_LW data. Finally, some general guidelines and recommendations are provided at the conclusion of the report so that the results from this study can be generally applied for design of MAS_RW and MAS_LW surveys at other locations.

2. METHODS

The primary goal of this research study was to experimentally evaluate key differences between MAS_RW and MAS_LW surveys, particularly with respect to source type, source offset, and receiver spacing. To accomplish the goals of this study, multiple methods were used to characterize three sites in southeastern Pennsylvania that represented a broad range of subsurface conditions. "Ground truth" conditions were estimated from seismic geophysical testing and were used to explore the role of field parameters using collocated MAS_RW and MAS_LW receiver arrays. The following sections discuss the sites selected for this study and the seismic geophysical testing performed at each site.

2.1. Site Selection

One of the objectives of this study was to compare Rayleigh and Love wave dispersion at sites with different stiffness profiles. In particular, sites where Love waves are likely to perform well were targeted as well as more "normally dispersive" sites where Rayleigh waves yield more straightforward fundamental mode curves. This would ensure the findings would be applicable across a broad range of subsurface conditions and would allow a better understanding of the role site condition has on optimal data acquisition parameters. It has been established that a thin soft surficial layer provides excellent sites conditions in which to perform MAS_LW (Eslick et al. 2008). Moreover, the existence of significant impedance contrasts between subsurface strata has also exhibited good responses to Love wave excitations (O'Neill 2004). Final site selection proceeded with identification of a couple of sites that fit within the parameters expressed by Eslick et al. (2008) and O'Neill (2004) and a final control site where "normal dispersion" takes place. Therefore, three types of subsurface profiles were targeted: (1) a site with a gradually increasing impedance/stiffness profile; (2) a site with soft-over-stiff impedance contrast at a deeper location; and (3) a site with a soft-over-stiff impedance contrast at a shallow depth. With regards to Love waves, the last two sites are more suitable for Love wave generation, and the first is the least-favorable to Love waves.

Selection of applicable sites proceeded by identifying probable locations based on geologic maps and any existing geotechnical/geological information (e.g., boring logs, monitoring wells, etc.). Initial exploratory seismic geophysical testing (typically seismic refraction and MAS_RW) was then performed to develop a working model of subsurface stratigraphy. This working model was categorized relative to the three desired site types. This process was repeated at over a dozen locations across southeastern Pennsylvania and southern New Jersey to select the most applicable sites. The site with a soft-over-stiff impedance contrast at the near surface proved the most elusive to locate. Based on this selection process, these sites within southeastern Pennsylvania were identified for this study (Figure 4). Note that two of the sites are located very closely and are represented by the same point on the map.

2.1.1. Gradual Impedance/Stiffness Profile

The southern soccer field at the Ambler Campus of Temple University (Temple Amber Soccer; TAS) was selected to serve as the site where the subsurface profile stiffness gradually increases with depth (Figure 5). Fill material had been placed to elevate this site for drainage when the soccer fields had been constructed within the last decade. This shifted the location of rock to much deeper in the profile and provided a gradually varying stiffness profile from the overlying soils/unconsolidated sediments. Four monitoring wells exist at different locations on the site. The wells have different depths and all have 15.2 cm steel casings. Locations of three of the wells as well as their depth properties are presented in Figure 6 and Table 1.

2.1.2. Soft-Over-Stiff at Greater Depth

The area adjacent to the Skip Wilson baseball field at the Ambler Campus of Temple University (Temple Ambler Baseball; TAB) was selected as the site with a soft-over-stiff profile at greater depth (Figure 6). General geologic conditions were the same at this site relative to the TAS site, with sandstone and shale bedrock present at depth. The major difference was that no fill material had been placed at this site, which meant that the large impedance contrast between unconsolidated sediments and rock was located at a shallower depth than TAS. However, based on initial exploratory testing at the site, it was anticipated that the depth to this impedance contrast was much deeper than the 1.0 m minimum thickness recommended by Eslick et al. (2008).

2.1.3. Soft-Over-Stiff at Shallow Depth

The Mountaintop Campus of Lehigh University (abbreviated as MTC) located in Bethlehem, Pennsylvania, was selected as a site where a soft layer is underlain by shallow bedrock (Figure 7). Rock outcrops, shown in Figure 8, were observed at several locations across this site. Three locations at the site were manually investigated using a hand auger. Soil samples taken from the boreholes showed that the top soil consists of moist silty soil. At one location adjacent to the survey line, a very stiff layer was encountered at about 0.25 m, and at the other two locations farther away from the survey line, the depth of the same stiff layer was about 0.4 m. As stated earlier, an impedance contrast at a shallow depth (typically shallower than 4 m) provides a situation in which Love wave can properly be produced (Eslick et al. 2008).

2.2. Geophysical Testing

The geophysical testing methods used in this study included MASW using both Rayleigh and Love waves, seismic refraction (P-wave and S-wave), and downhole seismic testing. The seismic

refraction and downhole seismic test results were combined to develop an estimate of ground truth that would serve as the baseline for comparison to MAS_RW and MAS_LW. In the following sections, each geophysical method is introduced in terms of data collection and post-processing.

2.2.1. MAS_RW and MAS_LW Testing

2.2.1.1. Data Collection

Surface wave data was collected using a 24-channel Geometrics Geode® seismograph plugged into a field laptop. The Seismodule Controller Software (SCS) was used to record the raw waveforms using 4.5 Hz vertical component geophones for Rayleigh wave testing and 10 Hz horizontal component geophones for Love wave testing. Both Rayleigh and Love wave testing were carried out using three different receiver intervals (0.5 m, 1.0 m, and 1.5 m). Shots were recorded at consistent offset locations, including 1*dx*, 3*dx*, 6*dx*, 12*dx*, and 24*dx* (where *dx* is the geophone interval), on either side of each survey line. At each shot location, multiple hammer strikes (typically 4) were stacked to increase signal-to-noise ratio. To reduce P-wave energy contamination, opposite impacts were performed and recorded at both sides of the two horizontal impact plates (wooden and aluminum source). The sampling rate and the total record duration for each shot were 0.125 ms and 2.048 s, respectively.

2.2.1.2. Seismic Sources and Impact Plates

A sledgehammer (20 lb and 4 lb), and an ESS-MINI accelerated weight drop (AWD) from GISCO were used as seismic sources throughout this project. The 4 lb sledgehammer generated waves with higher dominant frequency ranges, which focused on the shallower parts of the subsurface. The frequency bandwidth of the signals produced by the 20 lb sledgehammer was lower than that of the 4 lb hammer, meaning that it was able to evaluate deeper strata. The ESS-MINI AWD is an electrically operated portable seismic energy source. It was mounted on a trailer hitch and operated by a 12 V_{DC} automotive battery. The steel hammer used during strikes weighs 23 kg. According to the manufacturer's data sheet, the hammer strikes the impact plate with an average velocity of 4.25 m/s and introduces 208 J of energy with every impact. Four elastomers attached to the hammer are pulled while the hammer is raised to its highest point. Once the hammer is released, the stored energy in the elastomers is released, causing additional acceleration. The AWD can perform strikes at 0, 15, 30, and 45 degrees from vertical (Figure 9). A 0 degree impact is used to produce Rayleigh waves and the other three inclined positions are used to generate Love waves.

All sledgehammer impacts in this study were coupled with the ground surface using some form of base plate. The base plate used in MAS_RW testing was a 0.3 cm x 0.3 cm x 1.25 cm thick

aluminum plate. Two different couplers were constructed for MAS_LW testing. The first was an aluminum impact plate inspired by Haines (2007) (Figure 10 – 12). It consists of two T-sections acting as the impact surface welded to a horizontal base plate at an angle. Two rails support the T-sections and 10 spikes are used at the bottom to provide coupling with the ground surface. Coupling was also improved by standing on the base plate during strikes. The other Love wave source coupler consisted of a 15.2 cm x 15.2 cm x 61.0 cm lumber post. Two galvanized caps were attached to both ends to serve as an impact surface and reduce impact damage. However, our experiences demonstrated that the lumber quickly deteriorates even with this countermeasure in place (Figure 13). Multiple lumber posts were constructed and used during this study while only a single aluminum Love wave coupler was used.

2.2.1.3. Data Processing

After surface wave data collection was completed at all test sites for this study (Figures 14 – 16), the raw waveforms were processed using the Geometrics SeisImager/SW software package. This software uses the phase shift method (Park et al. 1998) to transform the wavefields into an overtone image and extract dispersion information. After the dispersion images were developed, an initial estimate of the dispersion curve was automatically selected by the software after examining for the peaks in the accumulated energy at different frequencies. This automatic selection process does not differentiate between fundamental or higher modes as it merely picks the location of maximum intensity in the overtone image for a given frequency. To extract the fundamental mode dispersion curve, suggested points from the automatic process were cross-examined with theoretical dispersion curves computed for the ground truth models at the three sites using MATLAB coding. Data points of higher modes were filtered out from the records.

This selection process was then repeated for all the shot records of interest and multiple dispersion curves were extracted from the records for each site. Then, an averaging function was implemented on select subsets of dispersion curves to combine them into representative dispersion curves. At each site, all the dispersion curve data points from Rayleigh and Love waves, regardless of their offset/source/interval, were averaged and examined in a single figure. This allowed for an overall direct MAS_RW-MAS_LW comparison. Then, given the primary emphasis of this study to investigate the role of offset/seismic source/receiver interval on Love wave data, the dispersion curves data points were analyzed in three different "clusters": (1) averaged based on their offset locations, leading to 5 categories (i.e., 1*dx*, 3*dx*, 6*dx*, 12*dx*, and 24*dx*); (2) averaged according to seismic input source characteristics (i.e., aluminum horizontal source, wooden horizontal source, and AWD with three different angle configurations); (3) averaged based on receiver intervals (i.e., 0.5 m, 1.0 m, and 1.5 m). All the representative dispersion curves were also smoothed by applying a moving mean function that averages three adjacent data points to remove some of the spurious fluctuations resulting from combining multiple dispersion curves. This process was repeated for dispersion curves from all the sites.

In addition to processing the waveforms with the phase shift method and examining their dispersion information, the raw waveforms themselves were examined with respect to frequency content and signal-to-noise ratio (*SNR*). The relative contribution of different frequency components was evaluated by performing the Fourier Transform of the acquired waveforms. The power spectrum of the signal was then determined by squaring the Fourier amplitude normalized by the number of samples in the waveform. Similar in concept, the relative energy (Miller et al., 1986) was also determined by summing the squared Fourier amplitudes and used to evaluate the energy transferred to the ground surface from the different sources used in this study. Again, similar to the previous methodology for dispersion information, the power spectra and relative energy of Rayleigh and Love waves were determined based on averaging across multiple records collected at each site (for specifics see section 3 of the report). Love waveforms were further compared based on their offset, source type, and receiver interval. Similar analysis was performed for *SNR* of waveforms acquired with different source types, where *SNR* was directly calculated using Equation (2-1):

$$SNR = 20 \log_{10}(\frac{S}{N}) \quad (2\text{-}1)$$

where *SNR* is expressed in dB and S and N are the magnitude of signal and noise, respectively. To do so, first, a shot window was selected to ensure that the maximum signal generated by the impact was captured. This defined the maximum signal amplitude within the shot window. The same process was carried out to determine the maximum noise amplitude whereby a noise window was selected from the latter part of the recording after the shot signal has completely travelled through the receiver spread. The noise level of several records was then averaged and expressed as the representative noise level at that specific site. Despite the efforts to have consistent background noise during data acquisition at each site, the noise levels still fluctuated for different shot records, which could negatively bias the *SNR* estimates without the averaging described. A detailed explanation describing the actual recordings used to determine frequency content, relative energy, and *SNR* is presented in the discussion of the results in section 3 of the report.

2.2.2. Downhole Seismic Testing

The objective of downhole seismic testing (also called borehole testing) was to determine the subsurface velocity profile based on arrival times of compression (P) and vertically (S_V) and horizontally (S_H) polarized shear waves. Testing was performed at existing boreholes/monitoring wells at each of the sites (Figures 5 – 7). The material "sampled" by this method is located primarily in the general vicinity of the borehole (Figures 17 and 18). So it represents a more localized estimate of velocity. This information was combined with seismic refraction results to generate a ground truth model of velocity with which to compare MASW results acquired with Rayleigh and Love waves. Data collection and post-processing procedures are described in the following sections.

2.2.2.1. Data Collection

A 3-component borehole geophone (10 Hz) manufactured by RT Clarke was utilized to collect downhole seismic data in this study. The same Geometrics Geode seismograph used during MASW testing was used to record the downhole data. The downhole geophone was lowered to the bottom of the borehole (or to approximately 20 m when the bottom was deeper) and a clamping mechanism was enabled to couple the geophone to the side of the casing (or rock when the borehole was no longer cased). The downhole geophone used in this study does not possess an internal compass or a servo mechanism to rotate the horizontal component geophones to a particular azimuth. Therefore, it was impossible to have complete control over horizontal geophone orientation when the unit was lowered down into the hole. This would have little or no impact on P-wave testing, but it could degrade data quality for downhole S-waves since the horizontal geophone were not lined up with the polarization of the shots at the surface. As a countermeasure to this limitation, shots were performed at multiple offsets surrounding the boreholes to ensure that waveforms with sufficient quality and *SNR* could be extracted and used to determine arrival time from at least one of these shot locations. Additionally, multiple strikes were used to perform signal stacking and increase *SNR*. After data was collected at a given depth, the geophone was raised to a shallower depth and this process was repeated until all depths of interest were fully surveyed. The measurement interval typically depends on the required resolution, with closer spacing between measurements providing higher resolution for the site stratigraphy. However, a typical interval for measurements is not expected to be larger than 1.5 m or smaller than 0.5 m per ASTM D7400-17 recommendations. Subsequently, the depth interval selected for this study was 1.0 m.

2.2.2.2. Seismic Sources and Impact Plates

After the receiver was clamped, P-wave and S-waves were generated at the ground surface using the 20 lb sledgehammer. The 0.3 cm x 0.3 cm x 1.25-cm thick aluminum plate and the Haines (2007) horizontal aluminum base plate were used to couple the hammer impacts to the ground surface for P-waves and S-waves, respectively. Impacts were performed on both sides of the horizontal impact plate so that opposite polarization S-waves could be plotted to better identify the arrival times. The source was placed at a horizontal offset of approximately 1.0 m from the borehole location, which has implications on data processing as described in the next section.

2.2.2.3. Data Processing

The first step in data processing was to plot the raw waveforms against their respective depths and determine the time of first arrival of the corresponding waves. Travel distances are typically based on the assumption of straight ray paths between the source and receivers with no refraction

at layer interfaces. It is expected that the travel times will increase as the geophone is placed at deeper locations within the borehole. Additionally, the increase in attenuation resulting from the larger travel path reduces *SNR* and can increase the difficulty of picking first arrivals at deeper locations (Stokoe and Santamarina 2000). Signal stacking can counteract this issue to a certain extent and oppositely polarized S-waves can be plotted together to help clarify their arrival time.

Two conventional methods of downhole seismic data processing are available: (1) the direct method; and (2) the true interval or pseudo-interval method (Fernandez et al. 2008). In the direct method, the travel times are corrected at shallow depths to reduce the effects of source offset on the results. In such cases, the travel time must be multiplied by the cosine of the angle between the borehole and the direct line drawn from the source location to the examined depth. At depths greater than 10 times the offset this angle becomes small and the cosine factor is insignificant and can be neglected (Crice 2011). The corresponding P- or S-wave velocity of a given layer is calculated as the slope of the lines in the plot of corrected travel times versus depth ($H\text{-}t_c$):

$$V = \frac{\Delta H}{\Delta t_c} \tag{2-2}$$

where V is the desired velocity (i.e., P- or S-wave velocity), ΔH is the measurement depth interval, and Δt_c is the difference in the corrected travel time between two adjacent records. In the true interval method or pseudo-interval method, travel times are not corrected. Instead, the calculations are based on the length of the straight ray path from the source to the receiver. Velocities are determined as the ratio of the difference between the slant travel paths (L_{R1} and L_{R2}) of two consecutive measurements over the difference between the arrival times (Δt) of the same two records:

$$V = \frac{L_{R2} - L_{R1}}{\Delta t} \tag{2-3}$$

$$L_R = \sqrt{(\text{Source Offset})^2 + \text{Depth}^2} \tag{2-4}$$

This study followed the recommendations of ASTM D7400-17, which adopts the true interval method to estimate velocity.

2.2.3. P- and S-wave Refraction

Seismic refraction is considered the oldest method of near-surface seismic techniques that has been used widely for mapping the geometry of shallow geologic interfaces (Butler 2005). Similar to downhole testing, the methodology depends on picking first arrivals of body waves (both P- and S-waves), which means it is critical to accurately detect first arrivals on field records. When a generated body wave reaches the interface between a soft soil layer and a second stiffer layer, a portion of the wave energy will either be reflected back toward the surface, travel along the

interface, or transmitted into the second layer. Refraction occurs when the incoming ray path reaches the layer interface at a critical angle causing a portion of the initial wave to propagate along the boundary of the two layers. Then, the critically refracted wave acts as a new source for new secondary wavefronts. The secondary ray paths exit at the critical angle and return into the first layer and are measured by receivers at the surface. Seismic refraction "samples" a similar zone of the subsurface located within the array like MASW. The results from both P- and S-wave refraction were combined with downhole results to generate the ground truth model for the sites. The main reason for this is that refraction measurements are actually based on horizontal velocities (i.e., waves moving along the *horizontal* interface of two layers), but the outcome of refraction is an estimation of vertical velocities. This may introduce errors if the subsurface layers are significantly anisotropic (Milsom and Eriksen 2011). Details regarding data collection and processing are presented in the follow sections.

2.2.3.1 Data Collection

Data acquisition for MASW testing and seismic refraction is very similar. The main difference is that shot locations for retrieval of refraction waves are also located within interior of the geophone spread in addition to the exterior. Therefore, P- and S-wave seismic refraction testing in this study proceeded with the same hardware, configuration, and data acquisition parameters used to collect Rayleigh and Love wave MASW data, respectively. The longest receiver array (i.e., 1.5 m receiver spacing) was used at each site for the refraction testing. Closely-spaced shot stations can provide higher resolution. Therefore, shots were performed at every other geophone location within the array (i.e., channel 1, 3, 5, etc.).

2.2.2.2. Seismic Sources and Impact Plates

As with data acquisition hardware, the same MASW seismic sources and impact plates were used for seismic refraction. This primarily consisted of the 20 lb sledghammer and vertical impacts on the 0.3 cm x 0.3 cm x 1.25-cm thick aluminum plate and horizontal impacts on the Haines (2007) aluminum base plate. Impacts were performed on both sides of the horizontal impact plate so that opposite polarization S-waves could be plotted to better identify the refracted S-wave arrival times.

2.2.3.3. Data Processing

After data collection, the SeisImager/2D software package was used to select the P- and S-wave first arrivals from the collected refraction signals and further process the data for estimates of V_P and V_S. Due to their higher velocities and amplitudes, P-waves are typically easier to identify in the records whereas S-wave first arrivals can be quite challenging (Milsom and Eriksen 2011).

To facilitate picking the first S-wave arrivals, shots of opposite polarity were stacked. This prevented selection of the P-wave arrival in lieu of S-waves.

Data processing of refraction surveys can be accomplished by using a wide range of options from hand calculations to more sophisticated algorithms. However, the common methods that are usually employed are the time-term method, reciprocal time method, and tomographic method. A plot of first arrival time to different receivers versus distance serves as the basic input in all these methods. Before adopting any of the computational methods, it is recommended to examine the quality of travel times using the principle of reciprocity. This principle states that the travel time measured between the source and the receiver should be the same in the reverse direction. Data with reciprocal error of more than 5% should be treated with caution as the velocity models extracted from such data are likely to be invalid.

The time-term method, in its simplest form, assumes that all layers maintain constant velocities and horizontal interfaces, and utilizes a statistical linear least-squares approach to determine the depth of subsurface layers (i.e., refractors) from the given data. This method only requires layer assignments for each of the first break arrivals. The reciprocal time method (also known as ABC method, Hagiwara's method, and plus-minus method) generally requires more data, and therefore, more effort is involved in collecting refraction data when this method is being used. This method employs forward and reverse travel time data that have been acquired at receivers located between two shot points. It also requires more input from the user, and because of these reasons, it is recommended to use reciprocal time method when the results are expected to be as detailed as possible. In the tomographic method, an initial velocity model is created in a gridded 2-D dimension, and then rays are traced through the model, and theoretical travel times are compared to the measured travel times. After each comparison, the model parameters are modified, and this process is repeated until the difference between the calculated and measured times is minimized. With regards to the initial input model, some researchers have used the output of time-term inversion as the initial velocity model used in tomographic method (e.g., Dibiase 2004). In this study, the tomographic method was employed to invert the first arrivals.

3. RESULTS AND DISCUSSION

Once data was acquired and processed as described in the previous sections, estimates of the subsurface V_S and V_P profiles were developed as ground truth from downhole and refraction testing. This information was used in forward modeling to obtain theoretical Rayleigh and Love wave dispersion curves for each site. These dispersion curves were used to aid in selection of the fundamental mode dispersion curve from the experimental MASW data. These MASW results were then examined with respect to dispersion curve information, spectral content, relative energy, and *SNR* as a function of source type, source offset, and receiver interval.

3.1. Ground Truth Models

3.1.1. TAS Site

Figure 19 presents the results from the seismic refraction line and downhole surveys performed at TAS. The refraction line was collocated with the MASW surveys and the downhole survey was performed at MW2, which was the closest borehole to the MASW/refraction array. The two-dimensional (2D) refraction results were simplified into a one-dimensional (1D) velocity profile by taking the average velocity for each layer across the site. These results were then combined with the downhole profile by taking the time average velocity through each corresponding layer. The profile was further simplified into a fewer number of layers. As a rule of thumb, jumps of 30% or more were selected as the boundaries between two adjacent layers. The final V_S and V_P ground truth models are presented in Figure 20. The density of each layer was estimated at all sites by using the empirical relation from Ludwig et al. (1970):

$$\rho = 1.2475 + 0.399V_P - 0.026V_P^2 \tag{3-1}$$

where V_P is expressed in km/s. The TAS site demonstrates a gradual increase in stiffness from the ground surface to a depth of 25 m. No major contrast in layer stiffness was observed and the bedrock depth (based on a V_S = 760 m/s) was estimated at approximately 11.0 m below the ground surface. This site was expected to be the least conducive to Love wave generation given the gradual stiffness increase with depth and lack of a large impedance contrast at the near surface. The Rayleigh and Love wave dispersion curves for this velocity profile are shown in Figure 20. The layer model at this site is also summarized in Table 2.

3.1.2. TAB Site

Figure 21 presents the 1D and 2D velocity profiles obtained from the downhole testing at MW4 and seismic refraction surveys. As with TAS, the 1D profiles were developed as an average of the 2D profile throughout the site. The downhole and refraction results were combined and simplified into the ground truth model presented in Figure 22. As can be observed on this figure,

the stiffness of soil profile gradually increases until a stiff layer, bedrock, is encountered at a depth of about 5 m. As discussed previously, such an impedance contrast should typically be located at depths shallower than 4 m in order to provide optimal conditions for the generation of Love waves (Eslick et al. 2008). Therefore, it was expected that this site would be more favorable than TAS for generation of Love waves, but still less than ideal. The theoretical Rayleigh and Love wave dispersion curves were determined up to the second higher mode at this site (Figure 22). Table 3 summaries the velocity profile for the ground truth model at TAB.

3.1.3. MTC Site

Figure 23 presents the results from refraction and downhole testing at MTC. The P-wave data from downhole testing exhibited poor signal quality and was not combined with the refraction results to form the simplified V_P profile at this site. V_S models extracted directly from S-wave refraction and indirectly from P-wave refraction (assuming a reasonable Poisson's ratio) were averaged together to represent the refraction V_S profile. For only the top most 5 meters, these results were combined with the downhole profile because signal quality was quite poor below this depth and there is significant uncertainty in the downhole V_S results highlighted in Figure 23. The final ground truth velocity model for MTC is shown in Figure 24. The site has a relatively shallow stiff layer, most likely weathered bedrock, at a depth of approximately 1.5 meters. This layer represents a 150% increase in stiffness from the overlying surficial layer (Table 4). Additionally, V_S values indicative of bedrock (760 m/s) occur within approximately 3.5 m of the ground surface. Eslick et al. (2008) indicated from their experimental and theoretical studies that the ideal depths of the stiff layer to generate appreciable Love wave energy was between 1.0 – 4.0 m. The MTC site was therefore expected to serve as the site most favorable to Love wave generation. The theoretical Rayleigh and Love wave dispersion curves associated with the MTC ground truth velocity model are shown in Figure 24.

3.2. Effects of Source Offset

3.2.1. Dispersion Information

In this section, the effects of source offset (*SO*) on dispersion of both Rayleigh and Love waves will be examined. Particularly, the average Rayleigh and Love wave dispersion curves were examined for changes in general pattern of dispersion, minimum/maximum cutoff frequencies of the fundamental mode, and minimum/maximum retrieved wavelength. This allowed quantification of the effects of *SO* on surface wave generation and dispersion.

Figure 25 plots the average experimental Rayleigh and Love wave dispersion curves according to the source offset locations. A few points must be underlined prior to discussion of the results.

All the initial dispersion curves were extracted using the automatic selection process implemented by the SeisImager/SW software. However, a few measures were later implemented to ensure consistency in the outputs. First, limits were placed on the minimum and maximum retrievable wavelengths at each phase velocity to prevent spatial aliasing as discussed in Park et al. (2001). Second, in dealing with individual dispersion images, velocity reversals occurring at low frequency ranges were removed from the extracted data points. Such velocity reversals at low frequency ranges (large depth) are not naturally common and can be contributed to numerical artifacts, spurious noise, and logistical limitations such as the natural frequency of geophones. Finally, since the focus of the present study is effects on fundamental mode behavior, the selection of higher modes was avoided. This was accomplished through a careful comparison of the experimental dispersion information to theoretical dispersion curves from the ground truth models at each site by overlaying the two datasets. Points that appeared to belong to higher modes were filtered out from the curves and only the fundamental mode was retained.

An examination of Figure 25 reveals several important observations, some of which have been reported in the literature on previous occasions but primarily from a theoretical or numerical perspective. First, Love wave phase velocities tended to increase with farther offsets, especially at lower frequencies. It is believed that this change can be attributed to the near field effects, which causes a distortion in phase velocity estimation, especially for low frequency components (Park and Carnevale 2010; Foti et al. 2017). This tends to bias the phase velocity estimates to lower values for lower frequencies when closer source offsets are utilized. This pattern was much less consistent in the Rayleigh wave dispersion information.

Another key observation here is the difference in the presence of the fundamental mode in Rayleigh and Love dispersion wave curves at TAS (Figure 25a,b). As obvious in Figure 25a, Rayleigh wave testing at TAS suffered from a lack of fundamental mode data points in the frequency range of 22-56 Hz. This gap is manifested by straight lines connecting the data points below and beyond 22-56 Hz. Examination of the Rayleigh wave overtone images at this site showed that Rayleigh wave overtones acquired with a receiver spacing of 1.5 m are dominated by the presence of higher modes (see Appendix for all overtone images) over the same frequency range. However, evidence of Rayleigh fundamental mode become obvious at receiver spacing of 1.0 m. Love waves on the other hand provided a consistent fundamental mode in the range of 10-80 Hz. It has been reported in the literature that in many geologic environments, Love waves are less prone to higher mode excitation than Rayleigh waves, which can make interpretation of the Love wave fundamental mode much easier (Safani et al., 2005; Yong et al. 2013). This site is a promising example confirming this observation from the literature.

A third general observation is that Love waves provided smoother and more consistent curves than Rayleigh waves. This difference is clearer at sites with complex near surface irregularities. For instance, MTC contains shallow weathered bedrock with several complex fractures close to the near surface, most of which in the horizontal direction. A comparison of Figure 25e and 25f hows how more useful Love wave testing could be to interpret the site stiffness. The behavior exhibited by the Love wave dispersion curves in Figure 25 therefore demonstrates that the effects of source offset are more consistent. Changes in source offset can cause more scatter in the Rayleigh dispersion information, which can introduce a level of uncertainty not present in the Love wave data.

As mentioned previously, a detailed investigation was carried out by extracting the minimum and maximum frequencies and their corresponding maximum and minimum wavelengths, Table 5 summarizes these values for the three sites. Both Rayleigh and Love dispersion curves, with some fluctuations and inconsistencies, lose the high frequency range of their fundamental mode at larget source offsets (i.e., reduced f_{max}). This is again not surprising given that high frequency components attenuate at a higher rate with distance than lower frequency components. The attenuation of high frequency components corresponding to short wavelengths consequently limits the minimum depth of investigation.

Table 5 demonstrates that at the same offset location, Love waves tend to increase the maximum recovered wavelength from the dispersion images. This increase ranges anywhere from intermediate values (e.g., 10-15%) to extreme increases (e.g., 90%). However, caution should be practiced when dealing with these drastic increases as many of such dramatic changes have occurred at offsets close to the receiver array such as $SO = 1dx$. These short offsets are vulnerable to near-field effects. Moreover, dispersion data points from small offsets are usually used to complement the high-frequency end of the dispersion curves and are rarely used for their low frequency (long wavelength) content.

3.2.3. Near-Field Effects

It has been shown in several studies that at low frequencies (i.e., below 20 Hz), Love waves can have as much as 10% larger phase velocities than Rayleigh waves (Safani et al. 2005; Zeng et al. 2007; Mahvelati and Coe 2017). Therefore, at a given frequency in this range, the corresponding wavelength of Love waves would be larger. Also, as a rule of thumb, the minimum offset is usually taken as 25-50% of the maximum wavelength to avoid the effects of near-field (Park et al. 2002). Having these two points in mind, one can expect that the minimum offset for Love wave testing to avoid near-field effects would be slightly larger than that for Rayleigh waves.

The method presented in Yoon and Rix (2009) and Yoon (2005) was utilized to study the effects of source location on near-field effects of Rayleigh and Love waves. In this method, two normalized parameters are used to characterize near-field effects. The first normalized parameter is $\frac{x_1}{\lambda} = \frac{x_1 * f}{V}$ where x_1 is defined as the source-to-first receiver distance (Yoon 2005) and V is the phase velocity at frequency *f*. The second normalized parameter is the ratio V/V_{plane} in which V_{plane} is the plane phase velocity at frequency *f*. For negligible near-field effects $V \approx V_{plane}$.

From the TAS dataset, the Rayleigh waveforms collected with the 20 lb sledgehammer and receiver spacings of 1.5 m and 1.0 m were chosen to study near-field effects of Rayleigh waves. For Love waves, using the same dataset, records acquired with the horizontal aluminum plate and receiver spacings of 1.5 m and 1.0 m were selected for the same purpose. As a conservative estimate, offsets greater than 12 m were assumed not to be affected by near-field effects. In other words, waves generated from a source location of 12*dx* (with both *dx* = 1.5, 1.0 m) are assumed to be planar. Then, for all the data points, the unitless ratio of x_1/λ was calculated and the velocity was normalized against the benchmark velocities at 12*dx*. As can be noted on Figure 26, both Rayleigh and Love waves converge to a plane-wave situation with larger normalized distances. The Rayleigh wave sub-figure lacks data points at normalized distances greater than 0.3. The reason is that the Rayleigh dispersion curve from SO = 12*dx* contained only limited data points in the intermediate and high frequency ranges. However, the two sub-figures can still be interpreted. Assuming a velocity threshold of 90% (or above) for having a complete plane-wave situation, it can estimated that the ratio of x_1/λ in Rayleigh waves to meet this requirement is about 0.20 – 0.25. On the other hand, the same ratio for Love waves is slightly larger (approximately 0.25 – 0.30). This observation confirms that the minimum offset required for Love waves to avoid near-field effects is slightly longer than that for Rayleigh waves. Assuming a well-known rule of thumb relation between λ and spread length [$\lambda = (0.5 – 0.75)L$], it can be estimated that the minimum "safe" offset for Rayleigh waves is about $x_1 = (0.1 – 0.2)L$ which corresponds to an offset of 3.4 m – 6.9 m for a 24-channel system planted at 1.5 m spacing. For Love waves, this is approximately $x_1 = (0.13\text{-}0.23)L$, corresponding to 4.5 m – 8.0 m for the same data acquisition configuration. This also implies that all the records acquired at offset locations smaller than these ranges are adversely influenced by near-field effects.

3.3. Effects of Source Type

3.3.1. Dispersion Information

Figure 27 shows the average Rayleigh and Love wave dispersion curves based on the seismic source utilized during data acquisition. For Rayleigh waves, the comparison is made between a 20 lb sledgehammer impact on an aluminum plate versus the impact of the AWD on the same

plate. A few points should be highlighted. First, the stretch of fundamental mode dispersion curve from AWD shots at TAS (Figure 27a) is significantly smaller than that of the 20-lb sledgehammer. One reason for this observation is that due logistical and time constraints, the Rayleigh wave testing with the AWD at 0.5 m receiver spacing was not performed at this site. Therefore, the dispersion curve was not filled in with data from the smallest receiver interval, which would tend to emphasize higher frequency. The other contributing factor is that the overwhelming majority of Rayleigh wave overtone images collected with a receiver spacing of 1.5 m and 1.0 m were dominated by the first higher mode over intermediate frequency ranges. Given the focus on fundamental mode behavior in this study, all such data points were consequently removed from the dispersion curve. Examples of the overtone images with appreciable higher mode energy overlaid with the theoretical Rayleigh wave dispersion curves (dx = 1.5 m) is plotted in Figure 28a. Evidence of the fundamental mode begins to appear in the data acquired with 1.0 m geophone spacing (Figure 28b). Furthermore, some gaps in the fundamental mode Rayleigh wave dispersion curves can be identified in the frequency range of 26-52 Hz even when the sledgehammer was used. This was again the same range over which the accumulated energy was biased toward a higher and/or a combination of higher modes. However, compared to the AWD, a sledgehammer is producing more high frequency energy which increases the chances of having high frequency data. The tendency in overtone images toward higher modes was not the case for Love waves and the fundamental mode was present over a fair wide frequency range.

The right panels on Figure 27 show that using different source types did not meaningfully alter the low frequency end of dispersion curves. Specifically, the AWD and horizontal aluminum plate showed similar behavior despite the increase in energy offered by the AWD, which should emphasize lower frequency excitation. There is also a point that must be brought up regarding the horizontal wooden source. A careful examination of Figure 27b and Figure 27d reveals that the phase velocities from the wooden source are consistently lower than those of other source types. This discrepancy between the dispersion curves of wooden source and others becomes even stronger in Figure 27d. The horizontal aluminum source also exhibits similar behavior but it is limited to the results at TAS in Figure 27b. None of these observations were present in the MTC results. A potential explanation for the discrepancy in phase velocity data is that the wooden source is the only source of Love waves in which the impacts are performed at a pure parallel direction to the ground surface. In all other base plates, due to their inclination, a vertical component from impact is also introduced into the subsurface in addition to the horizontal component. It is possible that the presence and propagation of elastic waves from the vertical component of shots may contaminate the Love wavefield and bias the phase velocity to higher values. Also, note that except for MTC, dispersion curves collected with AWD at different angles of impact have demonstrated almost the same low and high cutoff frequencies. At TAS, the dispersion curves of the AWD with different angles tend to converge for frequencies beyond 12 Hz. At TAB, the frequency of convergence is at 20 Hz and it is at 32 Hz at MTC. The

minimum and maximum retrieved frequencies and wavelengths from the dispersion curves of different source types are summarized in Table 6.

3.3.2. Frequency Content

The frequency content of the input surface waves is related to what appears on the dispersion images. It has been long known that different source types have characteristic frequency responses and can therefore target different frequency ranges in the dispersion curve. Given some of the disparities highlighted in the previous section, it was important to examine the effects of different source types on the frequency content of the raw signals without transforming them into the dispersion image space.

Figure 29 plots the Rayleigh and Love wave power spectra collected with different source types at each site. The left panel represents the spectral content of Rayleigh waves and the right panel is that of Love waves. All the spectra have been extracted from waveforms acquired at source location 6*dx* with the *dx* equal to 1.5 m. The amplitudes in this figure were normalized with respect to the maximum observed power spectral density at a given site. Also, all the curves were smoothed by taking a running average of seven data points across each frequency bin (i.e., 3 points backward and 3 points forward).

As expected, the vertical impacts of the AWD provided more power than impacts of the 20 lb sledgehammer. However, the two seem to offer the same frequency bandwidth with no major shifts in the frequency content. Similarly, the power spectra of Love waves produced with different angles of AWD are quite similar in bandwidth and peak amplitude. Interestingly, increasing the angle of impact did not consistently improve performance with respect to peak power spectral density. At TAS, the power spectral density increased with AWD angle, but at MTC this pattern was reversed. Also, at TAB, there are multiple peaks in the power spectrum for the AWD-15º impacts, which are indicative of the severe mode splitting occurring in the dispersion behavior at this site. A similar pattern can be observed in the power spectrum of Rayleigh wave using AWD at MTC (Figure 29e). The wooden source consistently demonstrated poorer performance. One major anomaly for the wooden source occurs at TAB (Figure 29d). At this site, the wooden source exhibited lower dominant frequency than the rest of the sources, which all are about the same shape and centered around the same dominant frequent.

3.3.3. Relative Energy

Relative energy provides an indication of the energy generated by an impact source and can be computed from the summation of squared values of Fourier amplitude spectra. Figure 30 contains the relative energies computed for shot records collected with different sources at an

offset location of 6*dx* when *dx* is 1.5 m (except for Rayleigh wave at MTC which is reported for the offset of 3*dx*). All the energy levels in this figure have been normalized with respect to the maximum energy recorded within that sub-figure.

For both types of surface waves, the increased power of the AWD impacts did result in more energy transfer to the subsurface. The Rayleigh wave energy from impacts of the sledgehammer ranges from 50% to 70% of the energy level of the AWD impacts. In Love waves, the wooden source offered the least amount of energy. Similar to the observation made for power spectra, impacts of AWD from different angles did not exhibit a consistent pattern, and the optimal Love wave generation angle varies from site to site. However, the overall energy levels did not differ drastically as the impact angle was changed. In fact, the minimum Love wave energy generation from impacts at different angles was approximately from 65% to 95% of the maximum energy level encountered with the different angles.

3.3.4. Signal-to-Noise Ratio (SNR)

Signal-to noise ratio (*SNR*), as the name suggests, demonstrates the general quality of the collected waveforms and is defined as the ratio of the signal power to the noise power. *SNR* was calculated for shot records collected with different source types at an offset location of -6*dx* and *dx* = 1.5 m. At a given site, the maximum signal amplitudes corresponding to different sources were all divided by a constant representative noise level as previously describe in section 2 of the report.

Figure 31 presents the *SNR* as a function of receiver location along the receiver spread when receiver spacing is 1.5 m and the source offset is 9 m, except for the Rayleigh wave record at MTC which had an offset of 4.5 m. Unsurprisingly, the *SNR* of Rayleigh wave records from the AWD is always greater than that observed for the 20 lb sledgehammer. This was indeed expected given the larger amount of energy introduced by the larger seismic source mass. The trend of *SNR* for Love waves appears to be more site dependent. At TAS, a clear distinction can be made between different sources with the wooden plate offering the least *SNR*, followed by the horizontal aluminum plate and AWD. At TAB, the *SNR* from all source types (except the wooden post) exhibited similar values. Finally, at MTC, the wooden plate again has the lowest *SNR*, and horizontal aluminum plate and different AWD configurations are the superior seismic source. The performance of the wooden source is not surprising given the way impacts are performed. Our experience has shown that a slightly inclined seismic source is much easier to work with when compared to a completely vertical plate. Confidence and control over the impacts is increased when an inclined plate is utilized than when the impact plate is located completely perpendicular with respect to the ground surface. This logically leads to more energy transfer with the other sources. However, it must be underlined that lower *SNR* does not

necessarily correlate to poorer quality of overtone images. In fact, the overtone images from the wooden source exhibited similar (and sometimes superior) clarity relative to the overtone images generated by the other sources.

3.4. Effects of Receiver Spacing

3.4.1. Dispersion Information

Finally, the effects of receiver spacing on the dispersion of surface waves was investigated by examining the patterns in the average dispersion curves shown in Figure 32. Perhaps, among the three key survey parameters, the receiver spacing had the most consistent influence on Rayleigh and Love wave dispersion curves. According to Figure 32, for both the Rayleigh and Love wave curves, shorter spreads generally resulted in lower phase velocities, especially at low frequency ranges. This observation is implicitly rooted in the fact that with shorter receiver intervals, the offsets are also scaled down resulting in shorter overall distances from source to first receiver. As discussed previously, near-field effects tend to bias the phase velocity to lower-than-actual values at low frequency ranges. Also, according to Table 7, using Love waves can potentially increase the maximum recovered wavelength from the dispersion curves. This is because at low frequency ranges Love waves show higher phase velocities. Given the relation between phase velocity, wavelength, and frequency, the wavelengths of larger phase velocities would be longer if the frequency is equal. As previously discussed for the TAS site (Figure 32a,b), the Rayleigh wave curves suffered from lack of data in the intermediate/high frequencies and consequently exhibited a gapped fundamental mode behavior (red and green curves on Figure 32a).

3.4.2. Depth of Investigation

A suite of inversions was carried out on the dispersion curve data to examine the effects of receiver interval on depth of investigation (Figure 33). The inversion was performed using a linear least-squares inversion scheme with a root mean square error (RMSE) of 5% set as the threshold of convergence. However, some of the inversions, particularly with the Love waves, did not meet this requirement. Figure 33 plots the inverted V_S profiles with different geophone intervals across the sites. On each sub-figure, the V_S profiles of Rayleigh and Love waves are bounded by dashed lines of the same color as the V_S profiles. These lines represent the limitations on the minimum and maximum resolvable depths of investigation and are determined according to the minimum and maximum wavelengths retrieved from dispersion curves (i.e., as a rule of thumb $d = \lambda/3$). Within the boundaries defined by wavelength limitations (dashed lines), both the surface wave types show generally good agreement with the ground truth models. Still, at TAB, the difference between the estimated V_S from surface waves and ground truth model increases (especially below 10 m) and surface waves appear to underestimate the true model.

This could be partly due to two reasons. First, the ground truth model is partially constructed according to the seismic refraction survey, which is technically another form of seismic survey, and it has been reported occasionally that seismic refraction may overestimate the true velocity model (Yong et al., 2013). Also, surface wave inversion often struggles at low frequency ranges due to insufficient number of data points. This can also introduce additional sources of error.

Generally, the Love wave results in Figure 33 tend to estimate larger V_S profiles than Rayleigh waves, especially over the top 5-10 meters. This was expected due to the seismic anisotropy that usually exists in earthen materials in which the material is often more "*competent*" in the horizontal direction that it is vertically. Since Love waves measure the horizontal V_S due to their horizontal polarization, they often travel at faster velocities relative to Rayleigh waves and their S_V dependency. However, this pattern reverses at larger depths (corresponding to longer wavelengths), and V_S derived Rayleigh waves are faster than those from Love waves (except in Figure 33g). The same relation between Rayleigh and Love waves was reported by Safani et al. (2005). One explanation is that the stiffness of soil/rock is directly proportional to its stress state. Deeper beneath the surface, the horizontal and vertical stresses increasingly diverge with the vertical stress becoming much larger that the horizontal stress. When deep enough, the state of stress can compensate for any horizontal discontinuity and/or weathering that could have caused the near-surface vertical V_S to be smaller than near-surface horizontal V_S.

The maximum depth of investigation is controlled by the maximum wavelength (λ_{max}) corresponding to the minimum interpretable frequency component on a dispersion curve. As seen on the dispersion images, Love waves exhibited increased wavelengths at low frequency ranges due to their higher phase velocities. These increases would manifest themselves into increased target depths. This was indeed the case in some instances in Figure 33. Note that this observation was dependent on site and receiver spacing. For example, Figure 33b and Figure 33e demonstrate situations where the V_S profile from inverting Rayleigh wave dispersion information resulted in the larger depth of investigation. However, when Rayleigh waves exhibited larger depths of investigation, the increase was typically not greater than 1.5 m. The improvements from Love waves often exhibited approximately 2.0 – 9.0 m of increased depth of investigation.

The minimum wavelength extracted from the dispersion curves affects the shallowest resolvable depth of investigation. In this regard, expect for Figure 33a, Rayleigh and Love waves exhibited insignificant differences (less than 0.5 m) in their minimum resolvable depth of investigation. In fact, for the most part, the minimum wavelength of the two overlapped entirely as shown on Figure 33b through Figure 33i. The results at TAS with dx = 1.5 m (Figure 33a) was discussed earlier with respect to the effects of receiver spacing on the dispersion information. The average Rayleigh wave dispersion curve for this site and receiver spacing lacked intermediate and high

frequency components. This resulted in reduced near-surface resolution and an increased minimum depth of investigation.

3.5 Summary

The preceding results highlight that source type, offset, and receiver spacing can play a major role in interpretation of V_S profiles resulting from MASW. There were some appreciable differences between the effects of these field parameters on Rayleigh versus Love waves. Most notably, Love waves were capable of resolving V_S to larger depths than Rayleigh waves due to higher phase velocity and correspondingly longer wavelengths. The longer wavelengths meant that the minimum offset required for Love waves to avoid near-field effects was slightly longer than that for Rayleigh waves. Variations in the source offset introduced appreciable scatter in the Rayleigh wave dispersion behavior but the Love waves seemed immune to this effect. Similarly, Love waves tended to more consistently excite the fundamental mode, while Rayleigh wave dispersion image were affected by the presence of higher mode energy. This made interpretation of the fundamental mode dispersion curves more difficult for Rayleigh wave and decreased confidence in their subsequent inversions. Consequently, the V_S profiles obtained in this study from Love waves generally agreed better with the ground truth models established based on seismic refraction and downhole testing.

4. ACKNOWLEDGMENTS

We would like to thank current Temple University Ph.D. student Alireza Kordjazi and former Temple University M.S.C.E. students Philip Asabere and Michael Senior for their assistance during field testing. We would also like to thank Dr. Laura Toran for her input regarding the location of the monitoring wells at the Temple University Ambler locations. GISCO provided the ESS Mini AWD source used in this study and their support for our research team is greatly appreciated. We would finally like to thank Dr. Muhannad T. Suleiman for logistical support at the Lehigh Mountaintop Campus.

5. FIGURES

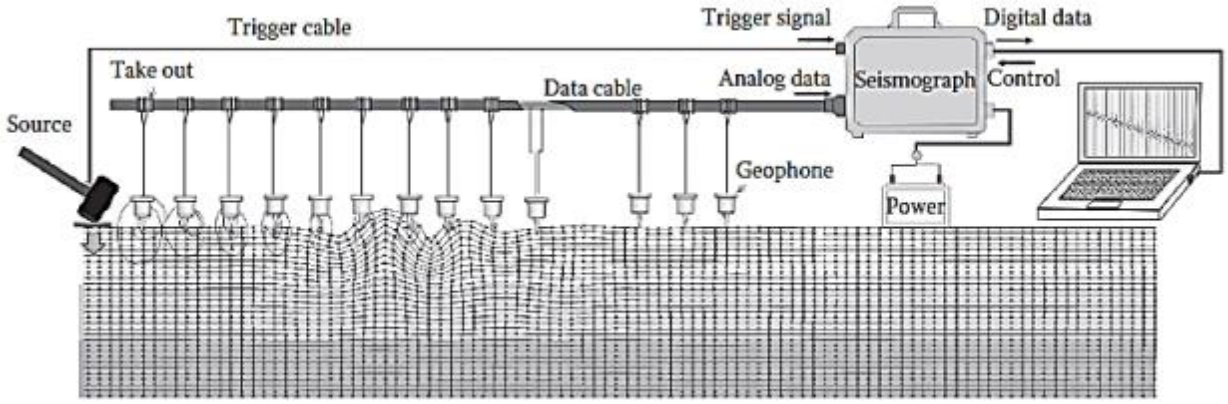

Figure 1. MASW field setup (Foti et al. 2015).

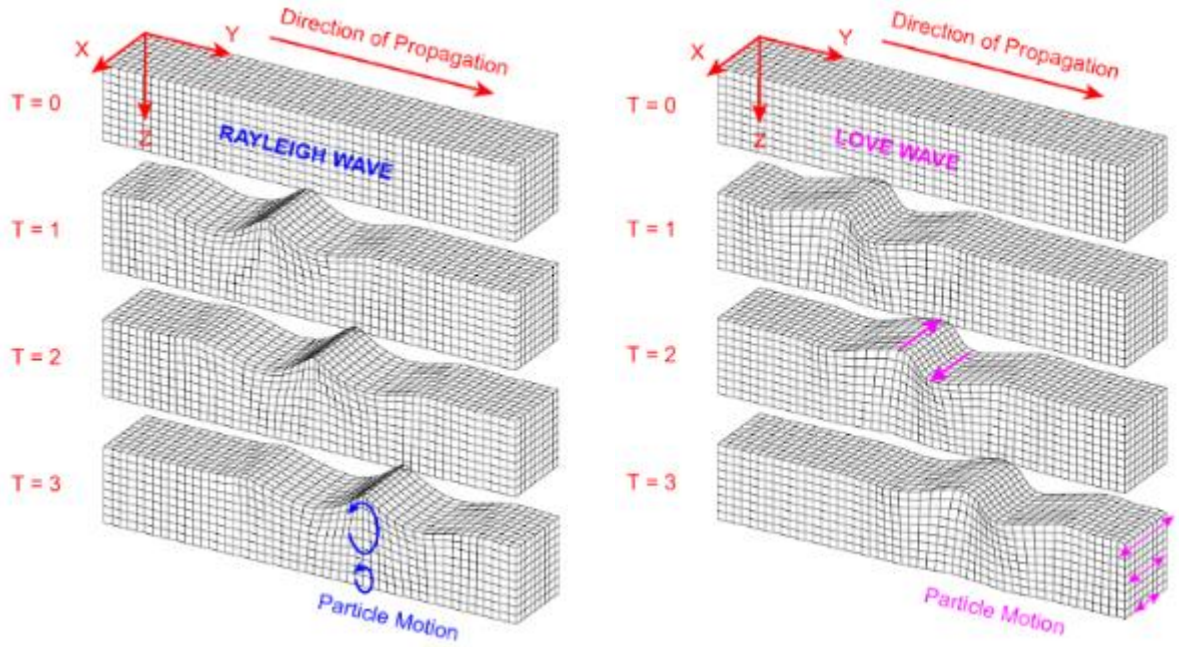

(a) (b)

Figure 2. Common surface waves for engineering applications: (a) Rayleigh wave; and (b) Love wave (Dal Moro 2015).

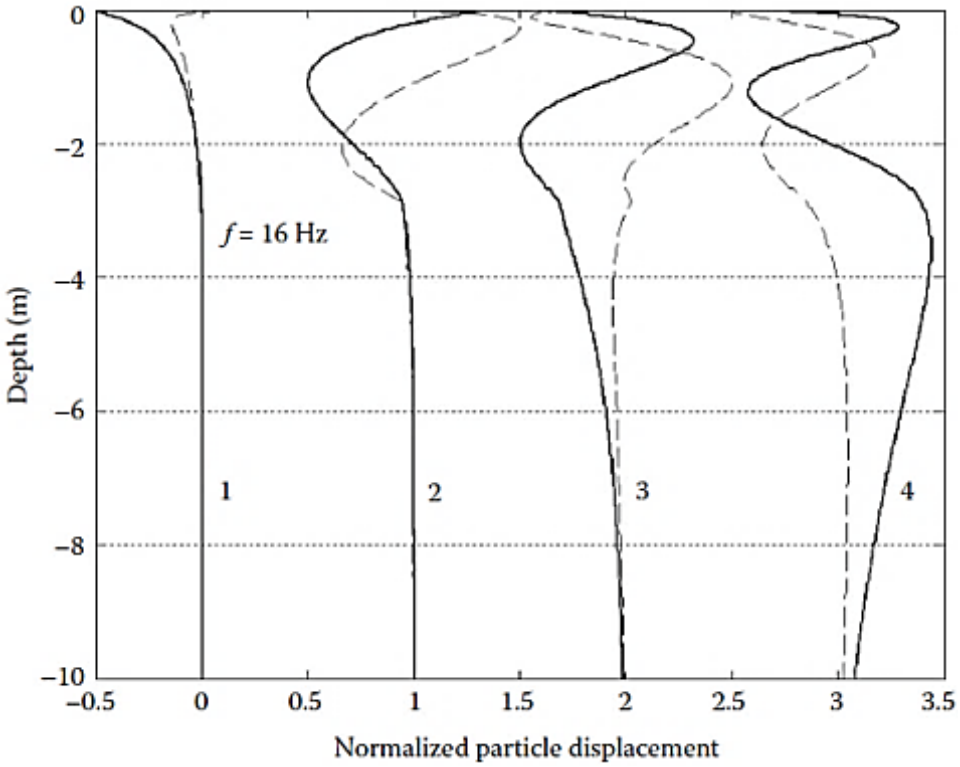

Figure 3. Four modes of Rayleigh wave displacement at f = 16 Hz in a layered medium (solid: vertical displacement and dashed: horizontal displacement) (Foti et al. 2015).

Figure 4. Survey sites (USGS).

Figure 5. TAS/TAB site locations and survey lines (Google Maps).

Figure 6. Monitoring wells at TAS site (Google Maps).

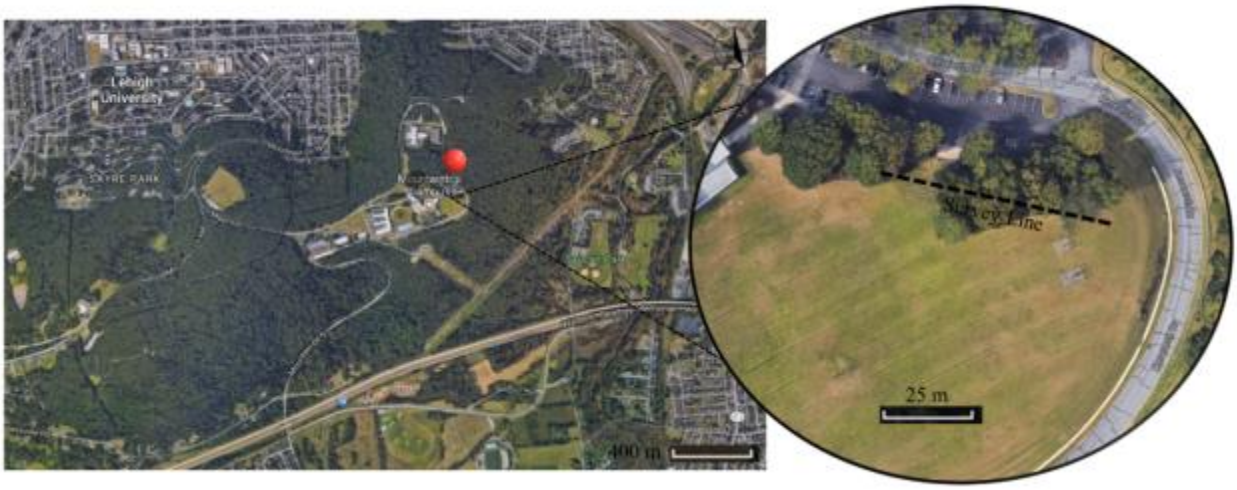

Figure 7. MTC site location and survey line (Google Maps).

Figure 8. Rock outcrops observed at MTC site.

(a) (b)

(c) (d)

Figure 9. GISCO ESS MINI AWD at different angles of operation: (a) 0º (vertical); (b) 15º; (c) 30º; and (d) 45º.

Figure 10. Haines (2007) aluminum Love wave base plate rail dimensions (all dimension in inches).

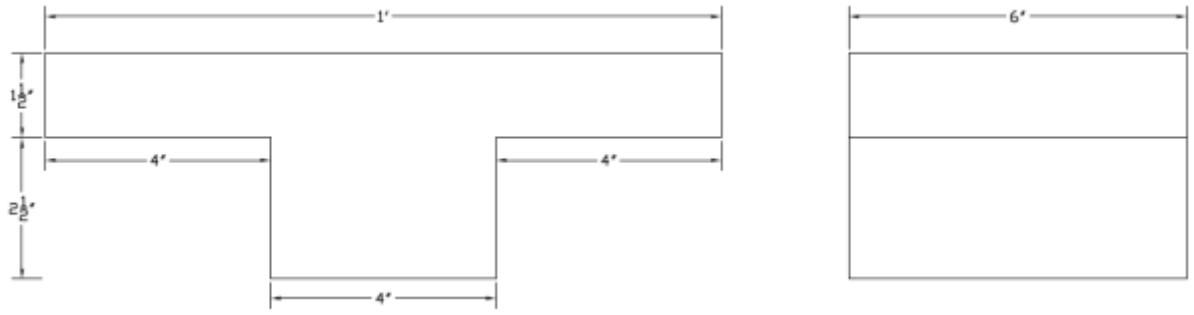

(a) **(b)**

Figure 11. Haines (2007) aluminum Love wave base plate T-section dimensions: (a) front view; and (b) side view.

Figure 12. Haines (2007) aluminum Love wave base plate.

(a) (b)

Figure 13. Wooden Love wave base plate: (a) 15.2 cm x 15.2 cm galvanized steel cap; and (b) wooden post.

Figure 14. Surface wave testing at MTC.

Figure 15. Surface wave testing at TAB.

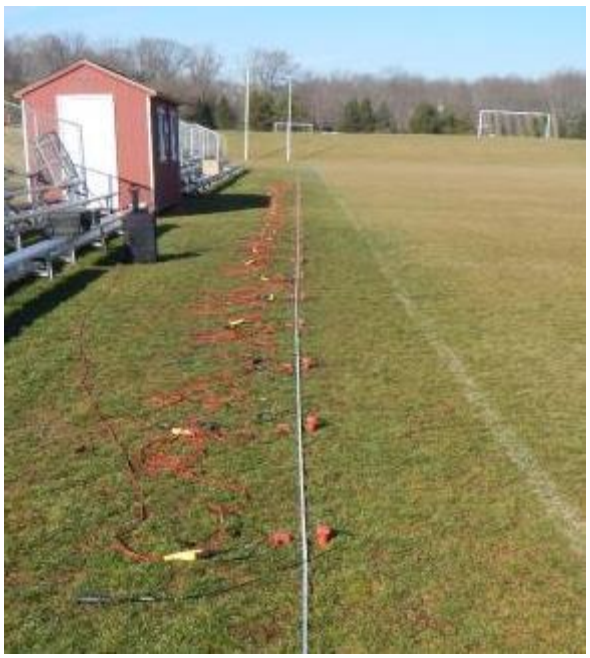

Figure 16. Surface wave testing at TAS.

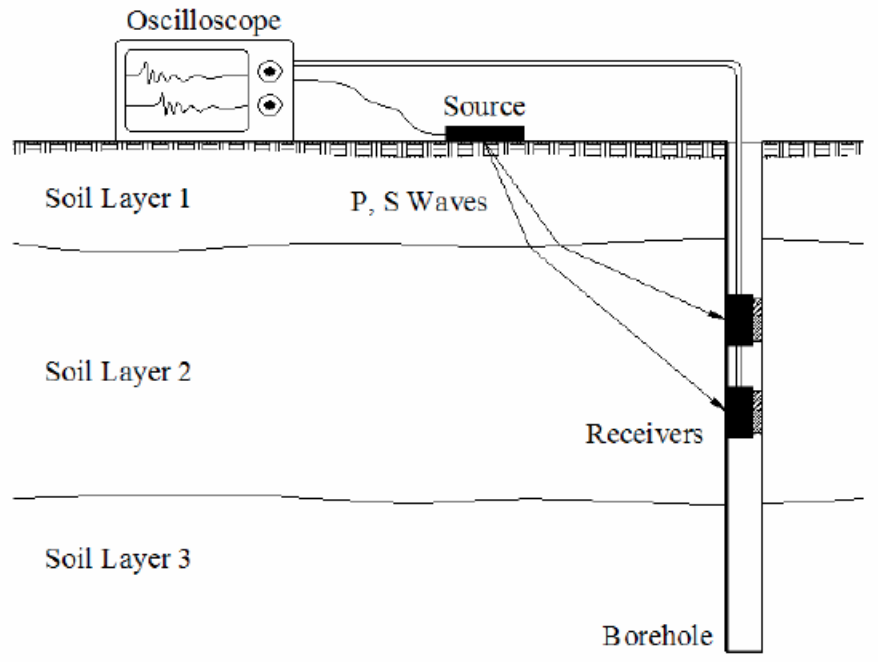

Figure 17. Schematic of downhole seismic testing setup (Fernandez et al. 2008).

Figure 18. Downhole testing at MW2 of TAS.

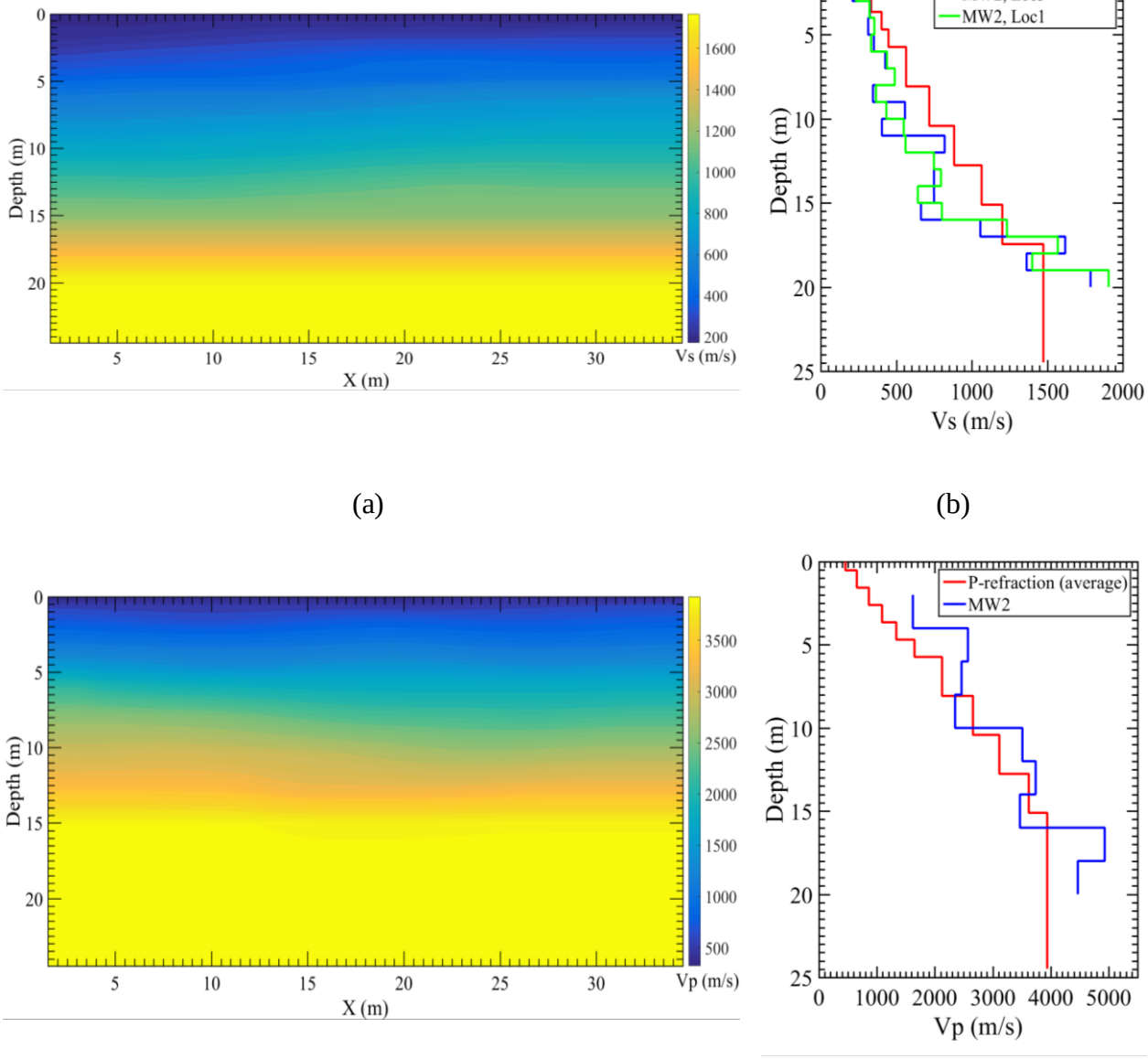

Figure 19. Refraction and downhole testing results at TAS : (a) 2D V_S profile from refraction; (b) 1D V_S profiles from refraction and downhole testing at MW2; (c) 2D V_P profile from refraction; and (d) 1D V_P profiles from refraction and downhole testing at MW2.

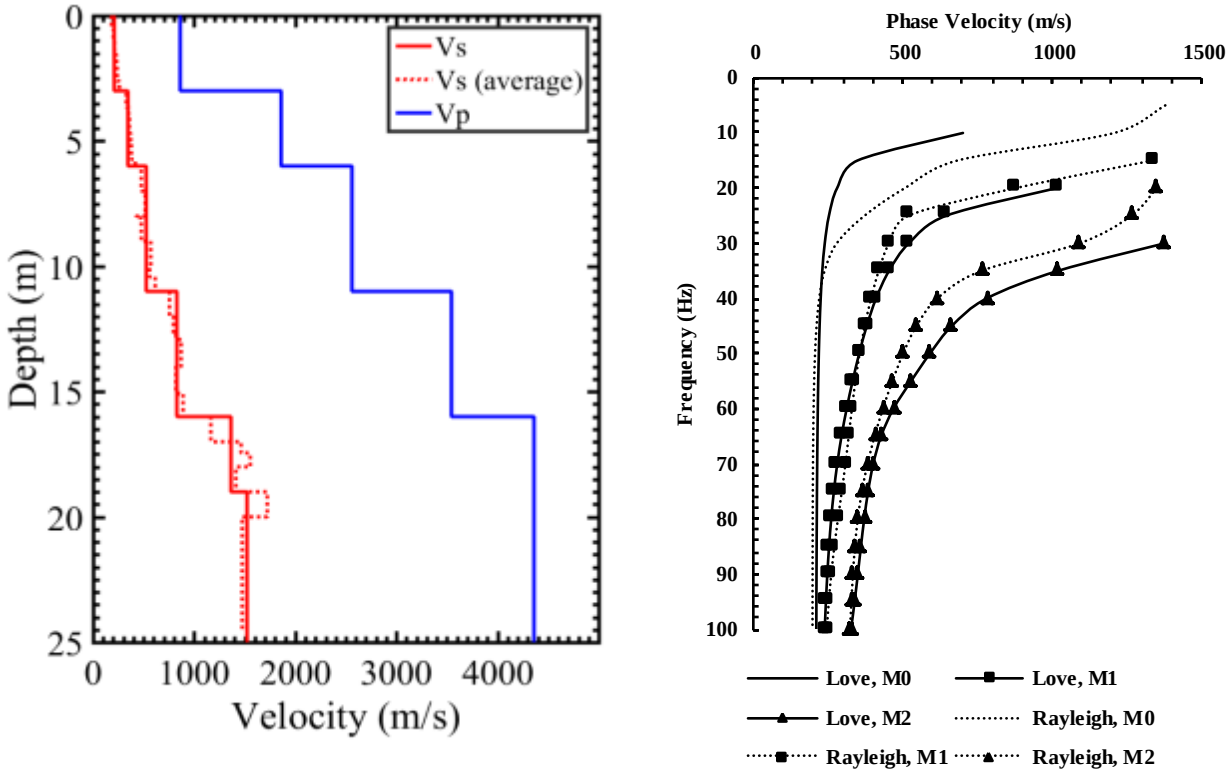

(a) (b)

Figure 20. Ground truth model at TAS: (a) V_S and V_P profile; and (b) Rayleigh and Love wave dispersion curves.

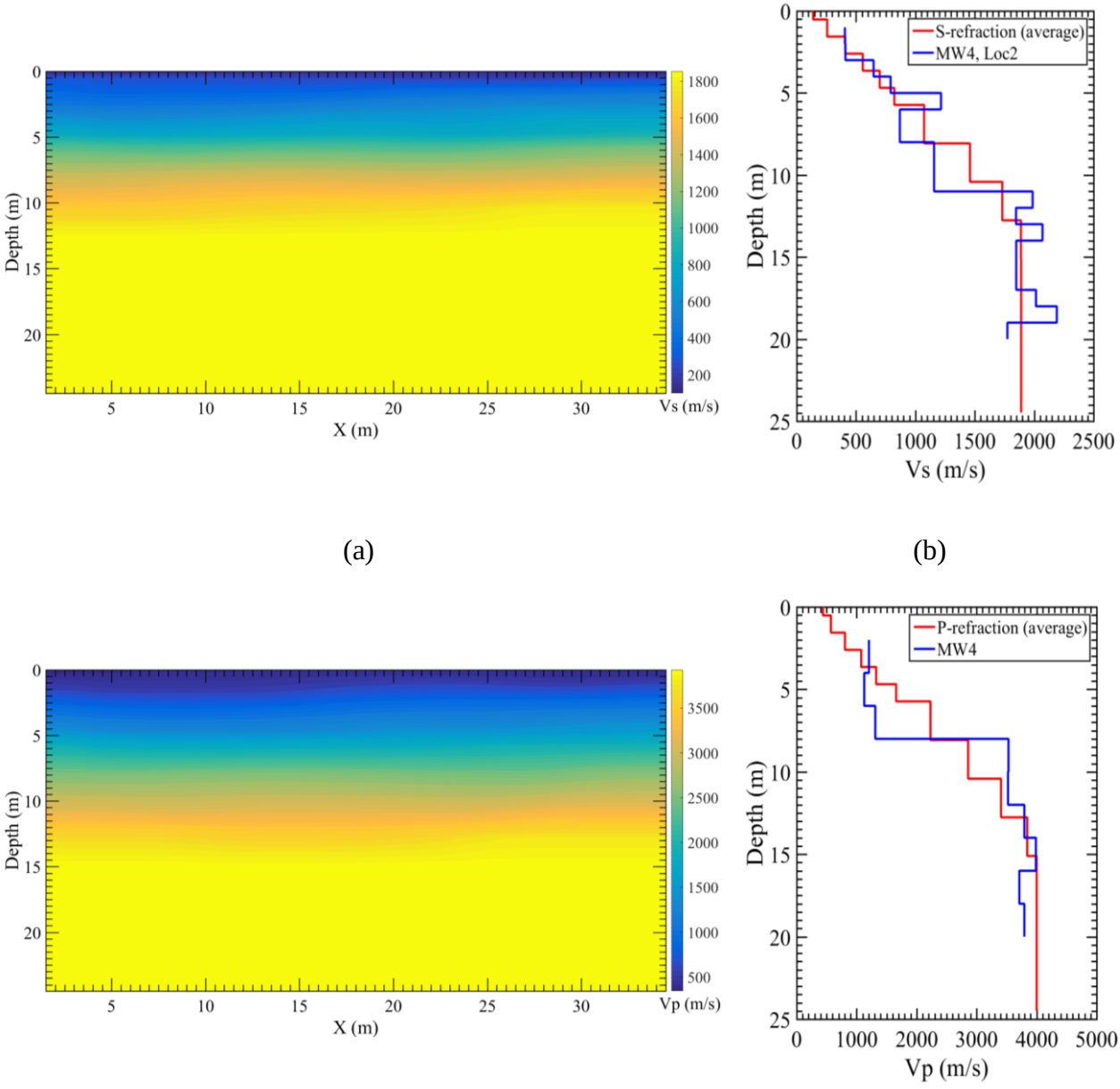

Figure 21. Refraction and downhole testing results at TAB: (a) 2D V_S profile from refraction; (b) 1D V_S profiles from refraction and downhole testing at MW4; (c) 2D V_P profile from refraction; and (d) 1D V_P profiles from refraction and downhole testing at MW4.

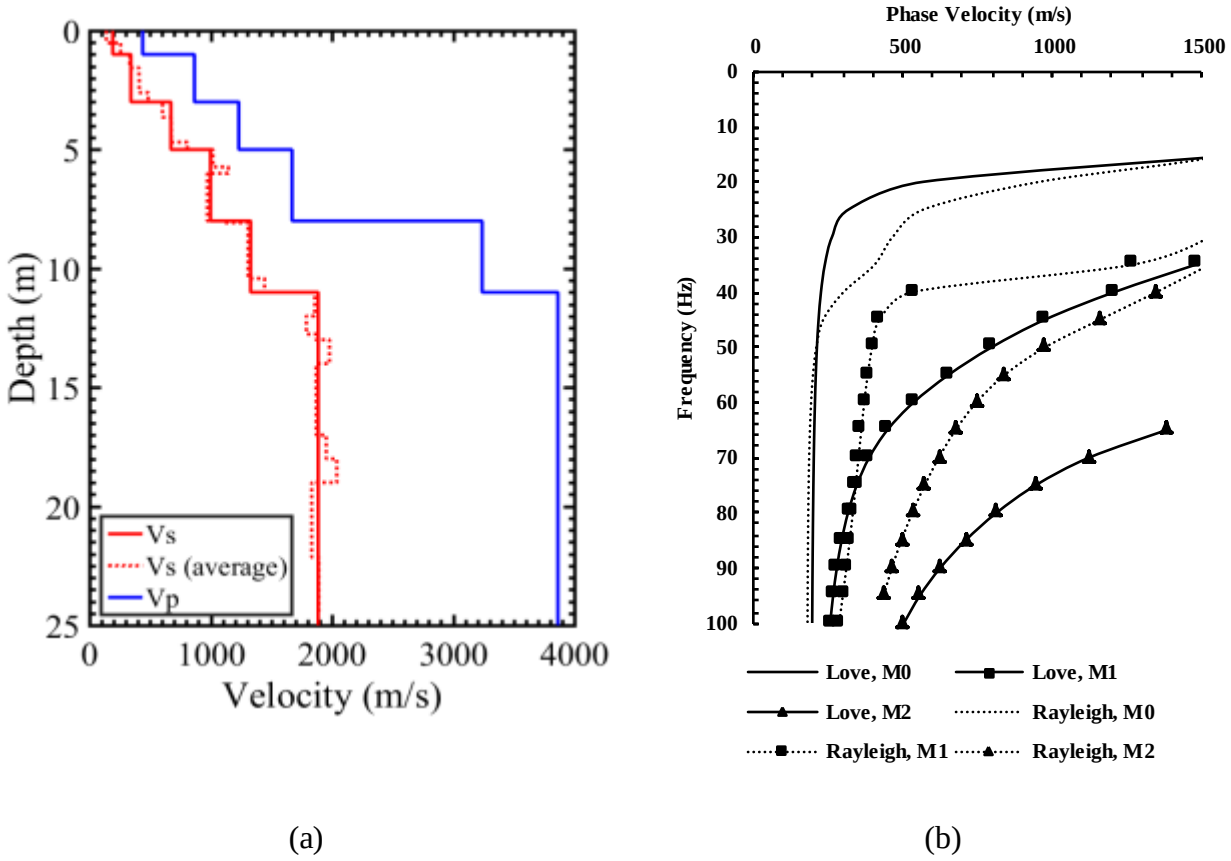

(a) (b)

Figure 22. Ground truth model at TAB: (a) V_S and V_P profile; and (b) Rayleigh and Love wave dispersion curves.

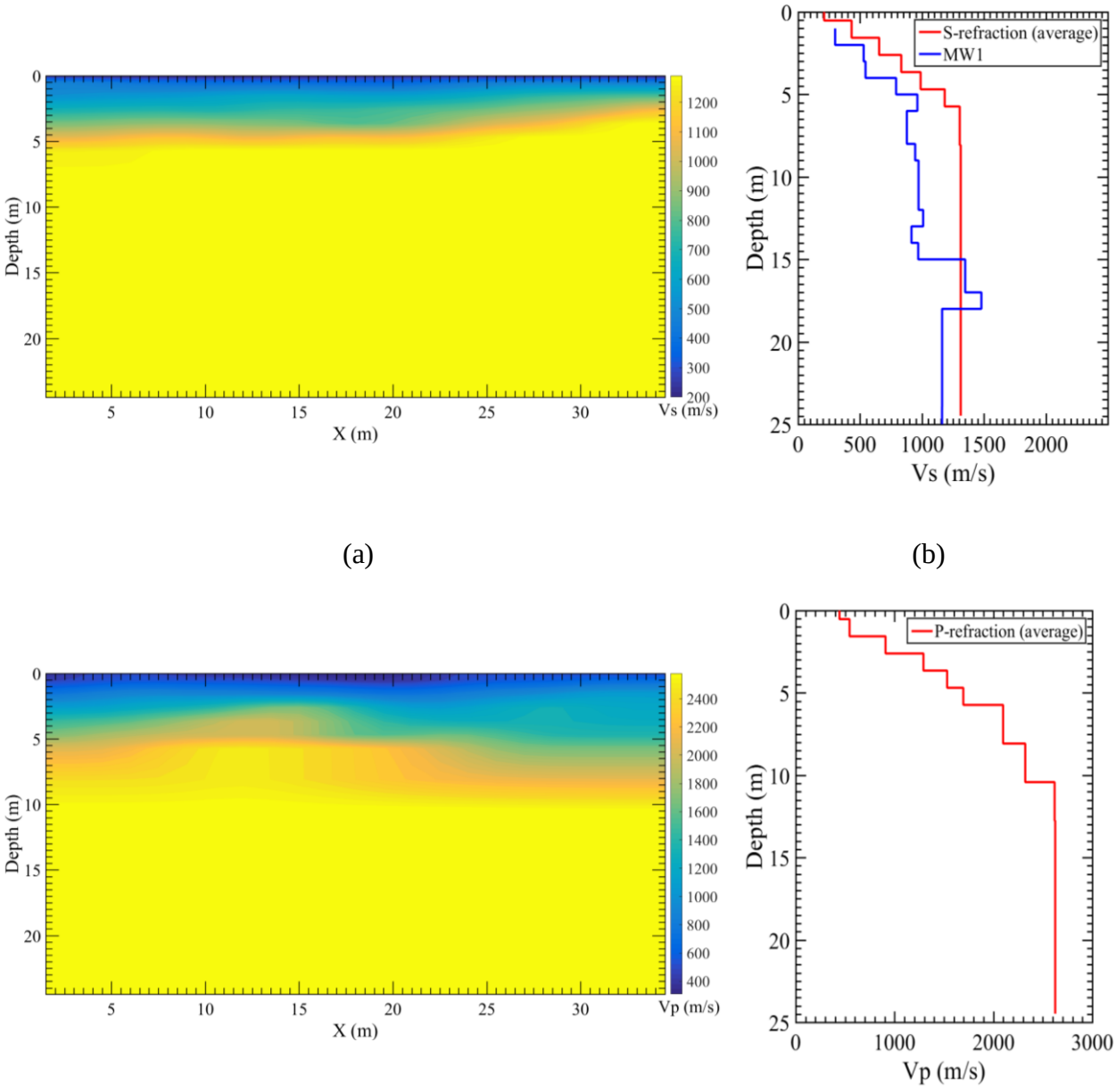

Figure 23. Refraction and downhole testing results at MTC: (a) 2D V_S profile from refraction; (b) 1D V_S profiles from refraction and downhole testing at MW1; (c) 2D V_P profile from refraction; and (d) 1D V_P profiles from refraction and downhole testing at MW1.

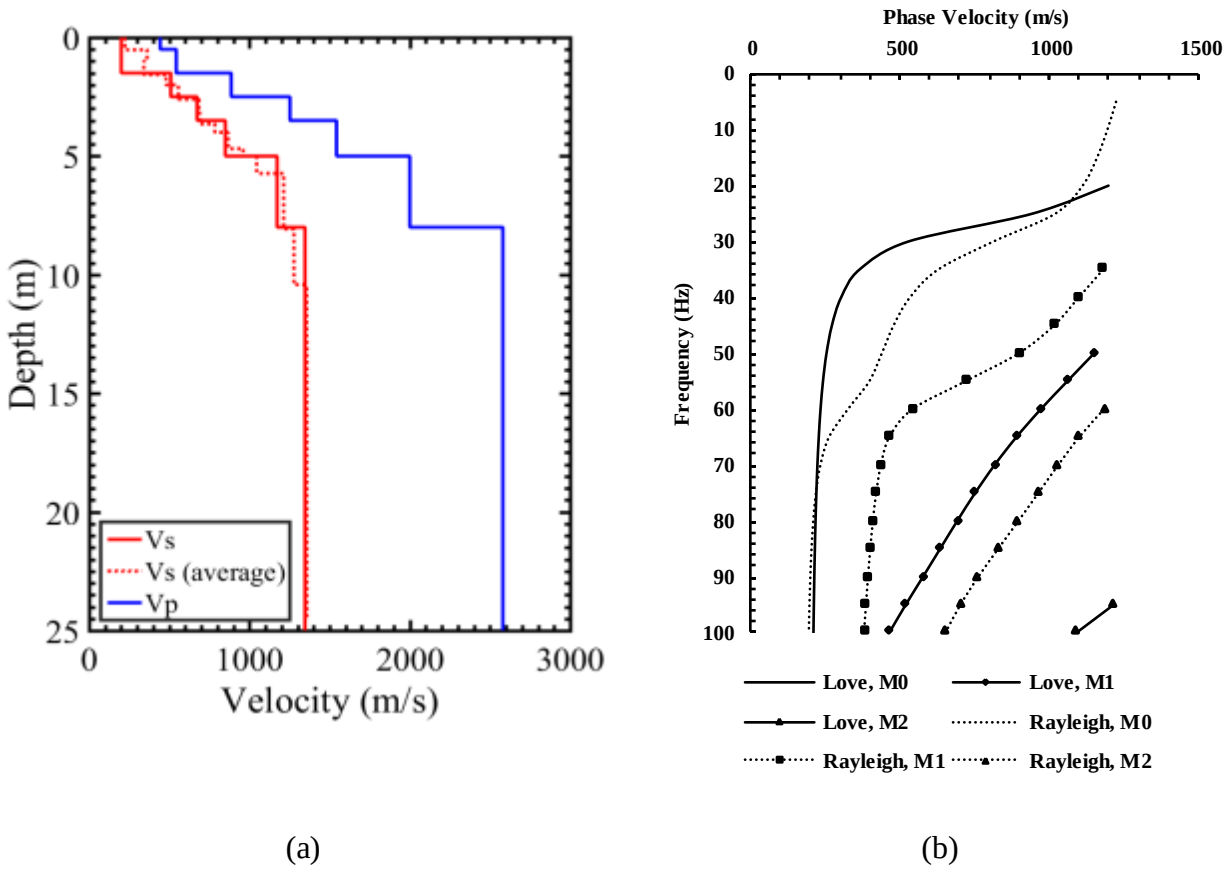

(a) (b)

Figure 24. Ground truth model at MTC: (a) V_S and V_P profile; and (b) Rayleigh and Love wave dispersion curves.

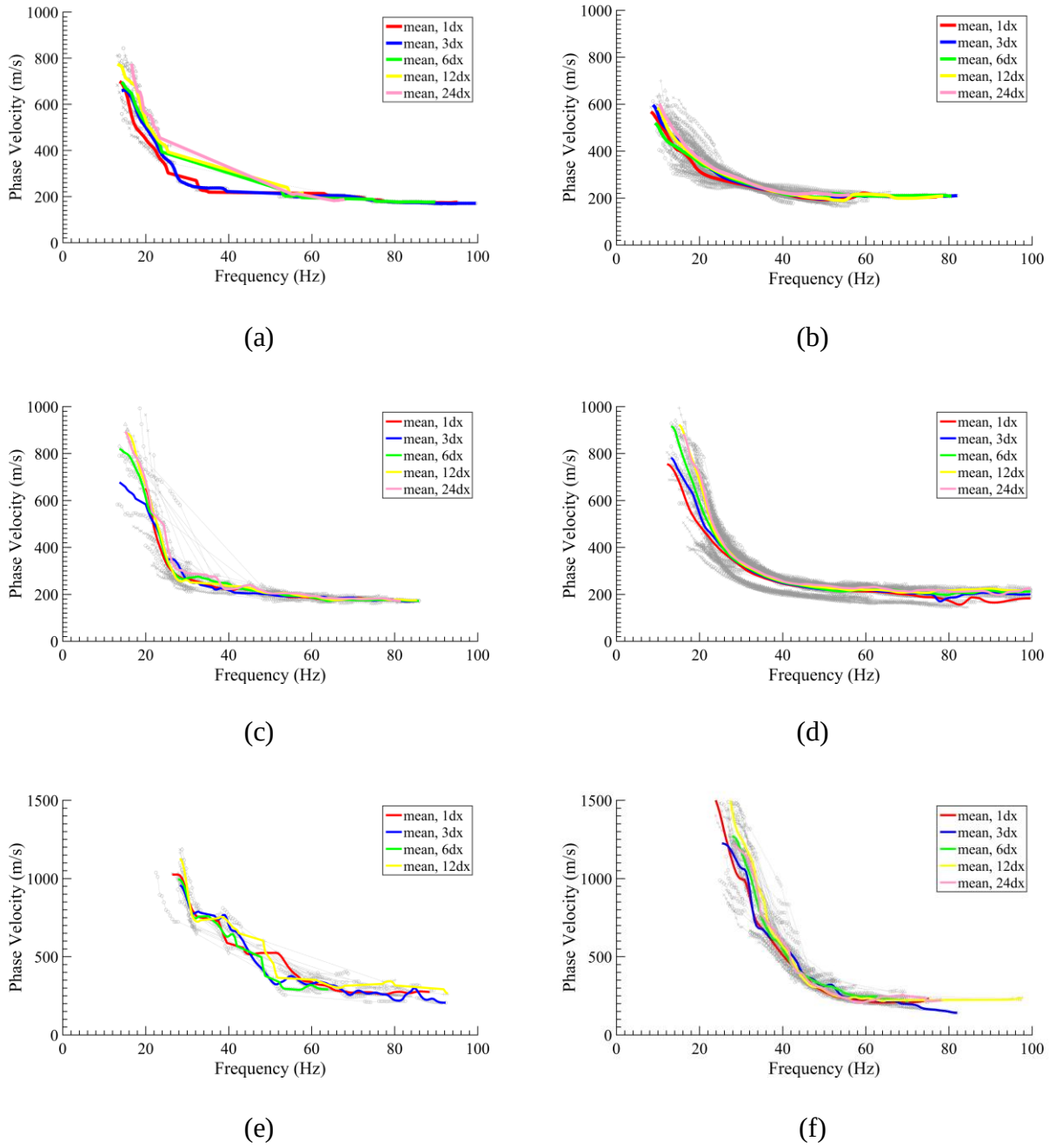

Figure 25. Dispersion curves of surface waves averaged based on source offset: (a) TAS Rayleigh; (b) TAS Love; (c) TAB Rayleigh; (d) TAB Love; (e) MTC Rayleigh; and (f) MTC Love.

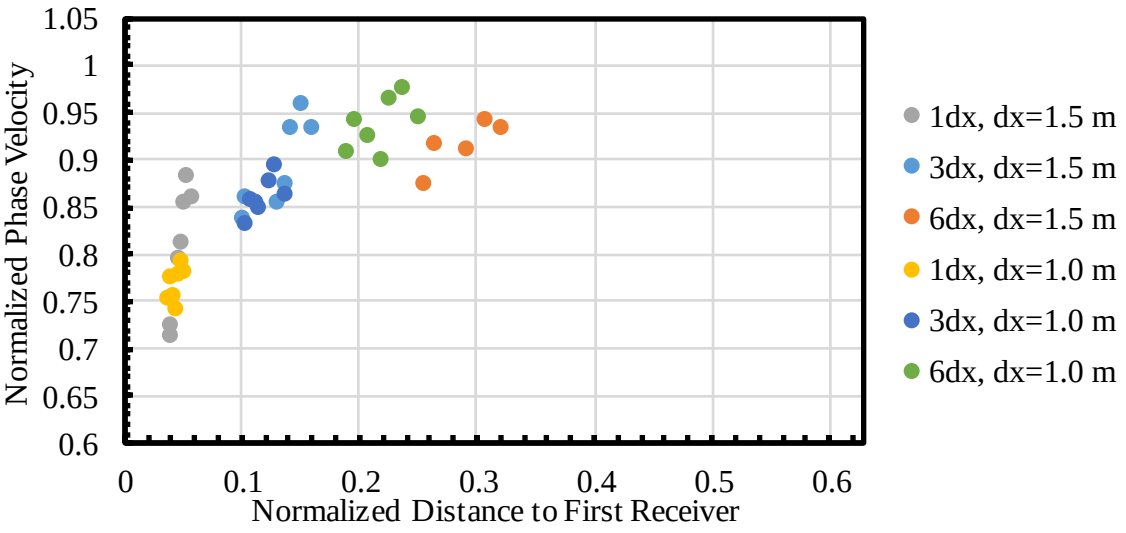

(a)

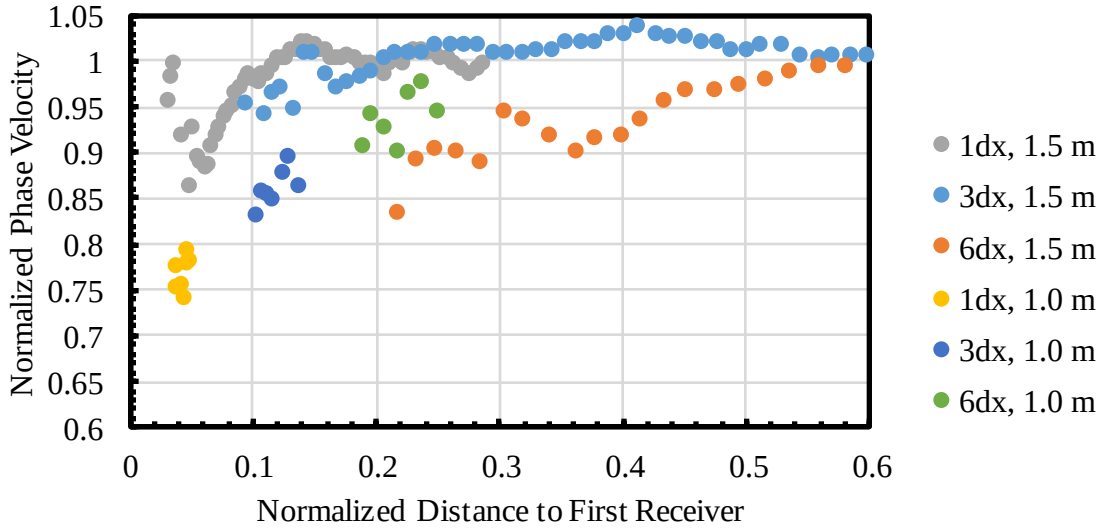

(b)

Figure 26. Near-field effects at TAS in terms of normalized parameters from field tests: (a) Rayleigh; and (b) Love.

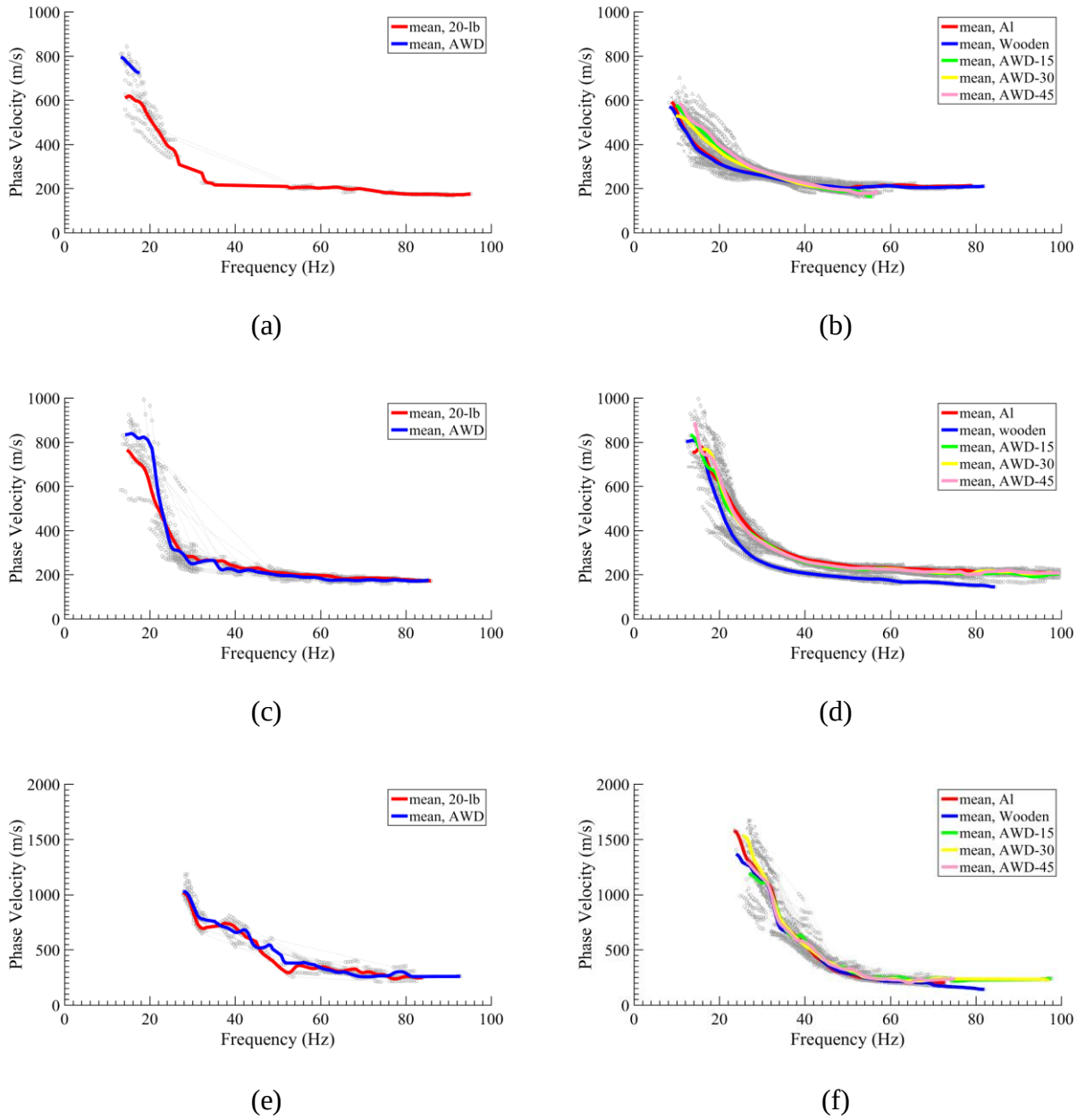

Figure 27. Dispersion curves of surface waves averaged based on source: (a) TAS Rayleigh; (b) TAS Love; (c) TAB Rayleigh; (d) TAB Love; (e) MTC Rayleigh; and (f) MTC Love.

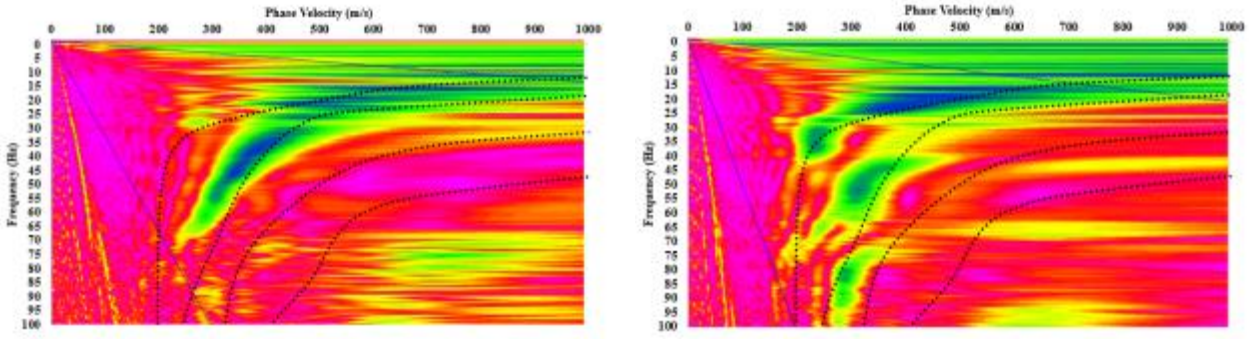

(a) (b)

Figure 28. An example of Rayleigh wave overtone images at TAS: (a) *dx* = 1.5 m; and (b) 1.0 m.

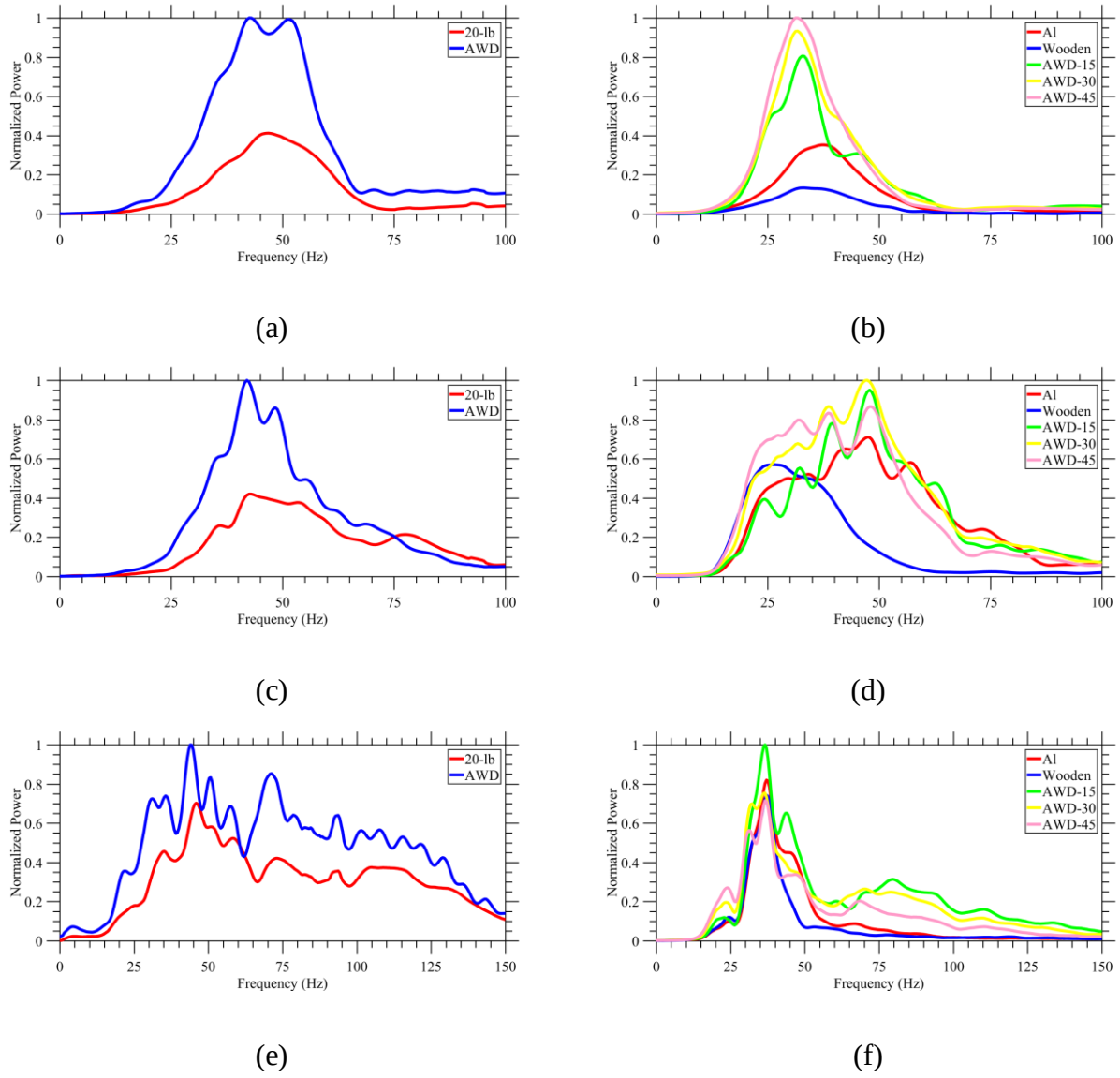

Figure 29. Power spectra of surface waves averaged based on source: (a) TAS Rayleigh; (b) TAS Love; (c) TAB Rayleigh; (d) TAB Love; (e) MTC Rayleigh; and (f) MTC Love.

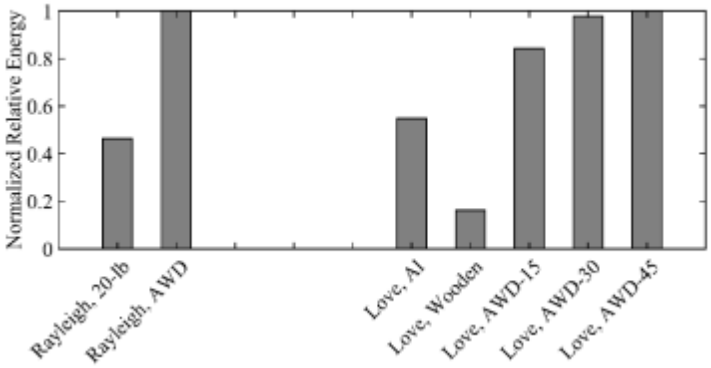

(a)

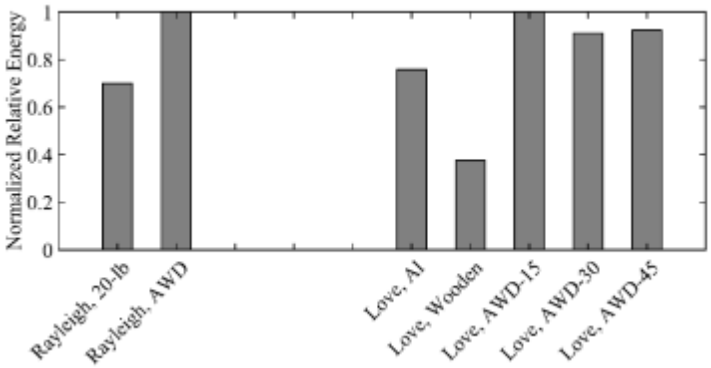

(b)

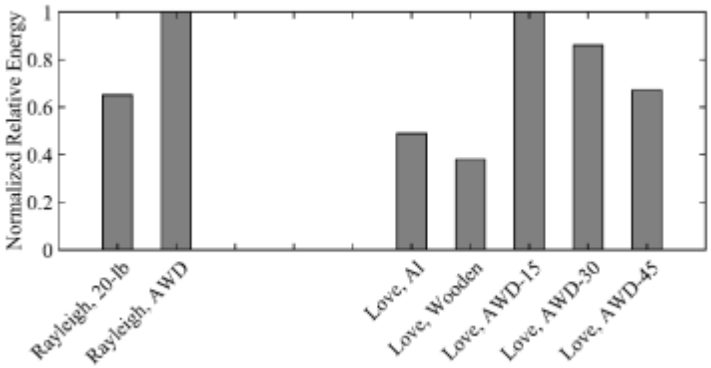

(c)

Figure 30. Relative energy of records collected with different source types: (a) TAS; (b) TAB; and (c) MTC.

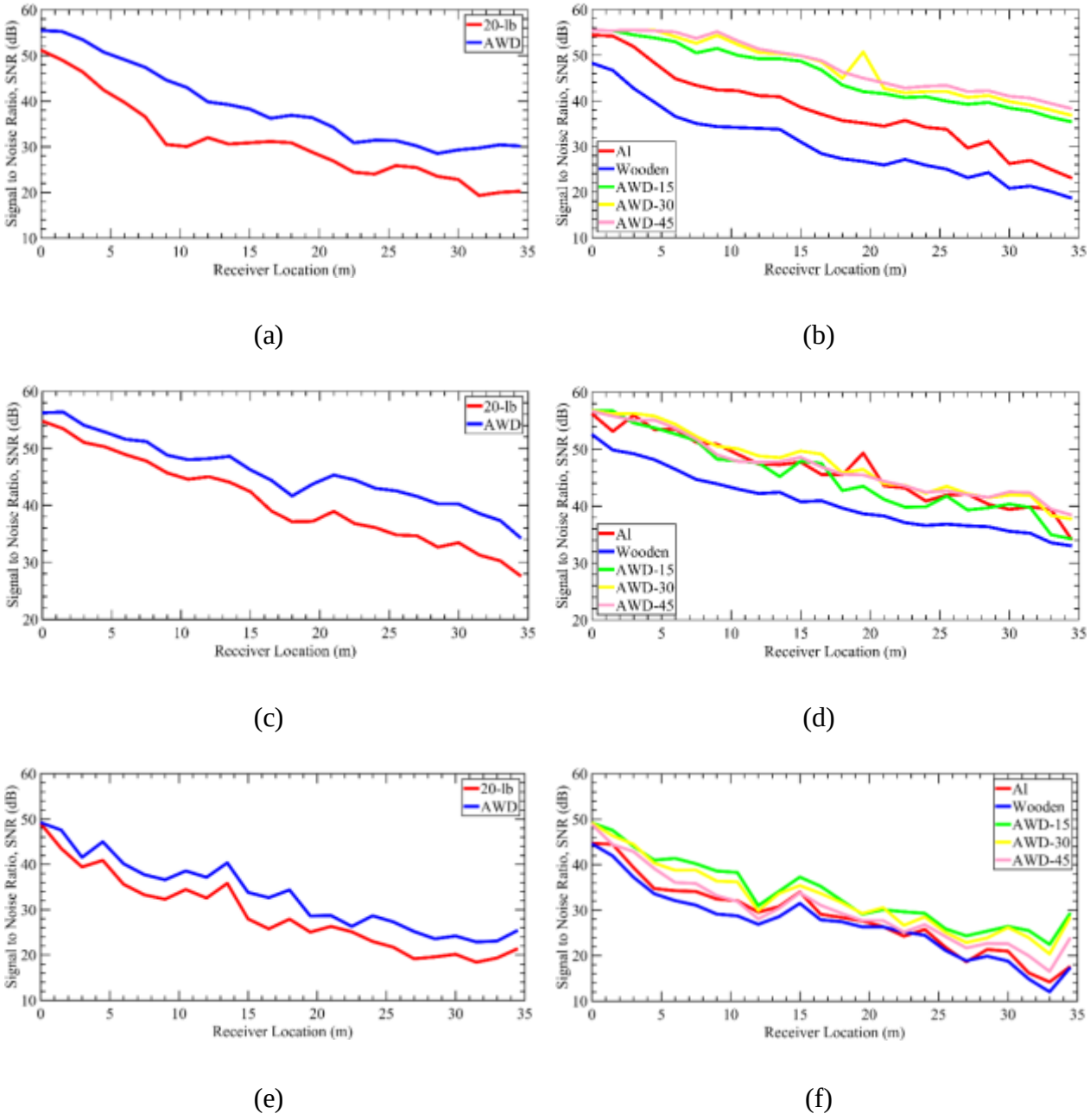

Figure 31. *SNR* versus distance for Rayleigh and Love waves: (a) TAS; (b) TAB; and (c) MTC.

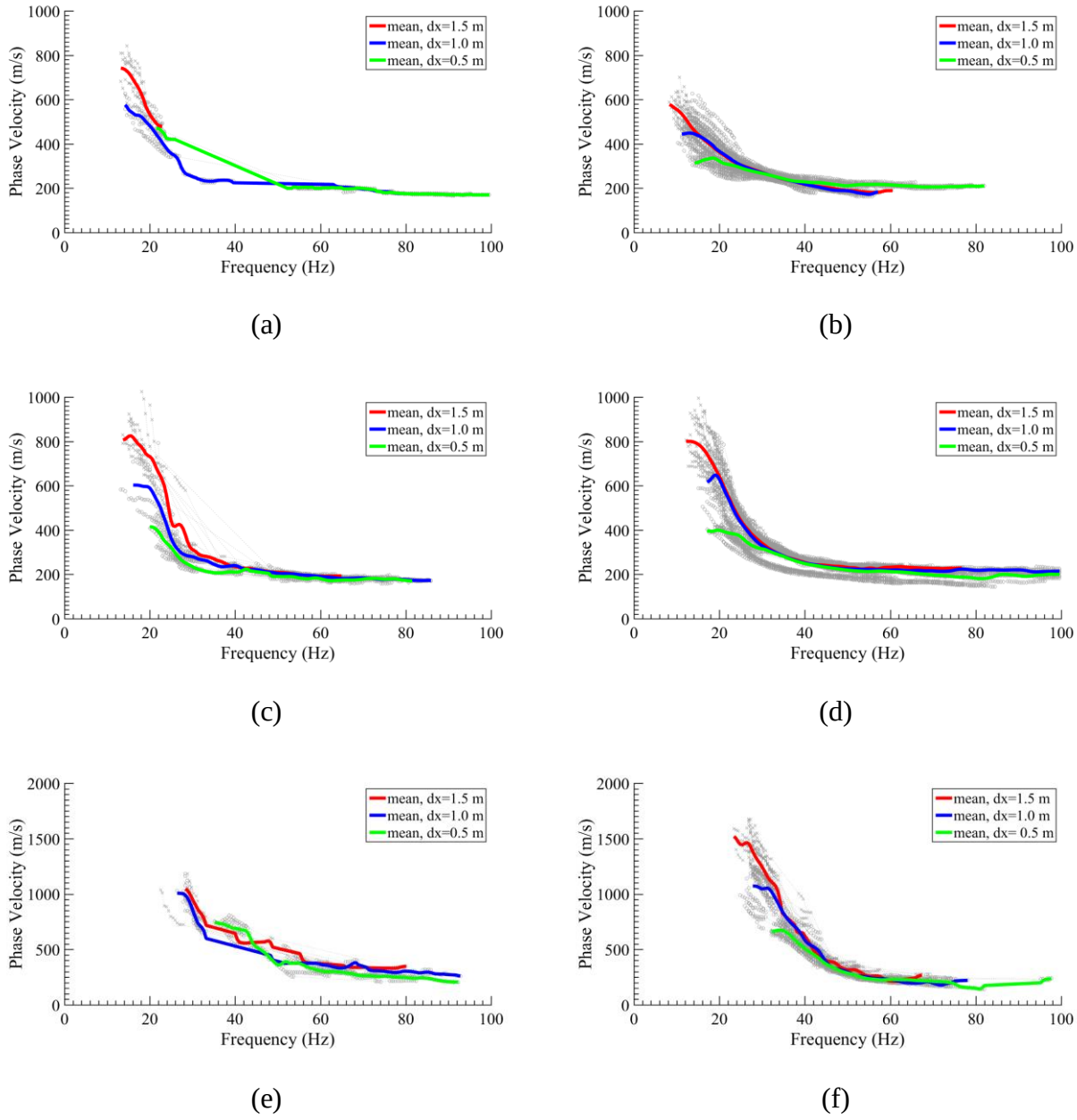

Figure 32. Dispersion curves of surface waves averaged based on receiver spacing: (a) TAS Rayleigh; (b) TAS Love; (c) TAB Rayleigh; (d) TAB Love; (e) MTC Rayleigh; and (f) MTC Love.

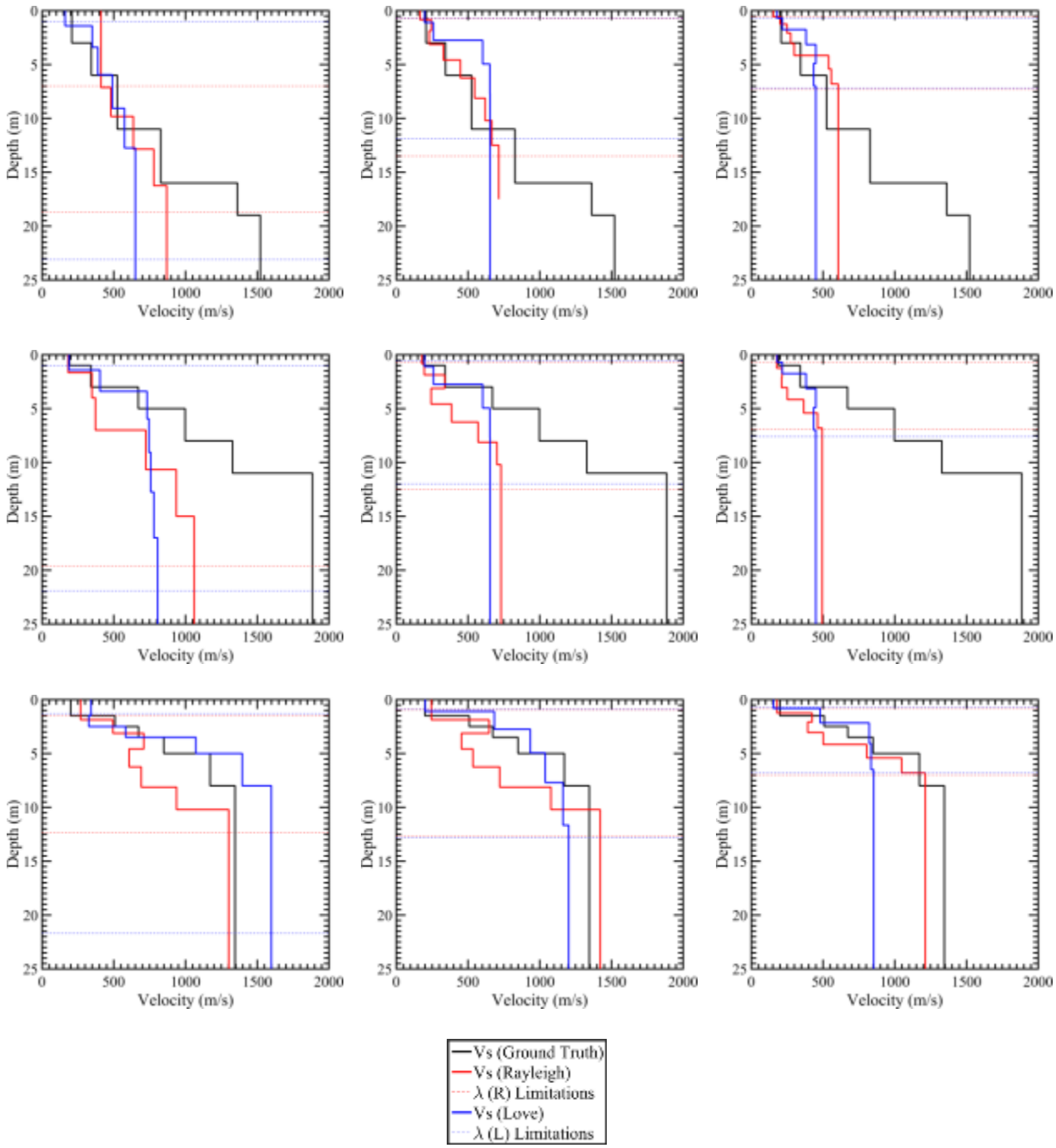

Figure 33. Inverted *Vs* profiles from MAS_RW and MAS_LW at the sites based on receiver spacing: (a) TAS *dx* = 1.5 m; (b) TAS *dx* = 1.0 m; (c) TAS *dx* = 0.5 m; (d) TAB *dx* = 1.5 m; (e) TAB *dx* = 1.0 m; (f) TAB *dx* = 0.5 m; (g) MTC *dx* = 1.5 m; (h) MTC *dx* = 1.0 m; and (i) MTC *dx* = 0.5 m.

6. TABLES

Table 1. Properties of the monitoring wells at TAS and TAB.

ID	Depth (ft)	Casing Type	Casing depth (ft)	Land Elevation (ft)
MW1	140	6 in steel	27.50	311.37
MW2	166	6 in steel	50.25	322
MW3	151	6 in steel	45.75	322
MW4	100	6 in steel	32.25	311.15

Table 2. TAS ground truth velocity model.

Layer	Depth (m)	Thickness (m)	Vs (m/s)	Vp (m/s)	ρ (kg/m3)
1	0-3	3	208	861	1572
2	3-6	3	344	1859	1899
3	6-11	5	525	2559	2098
4	11-16	5	828	3544	2335
5	16-19	3	1363	4360	2493
6	>19	-	1522	4360	2493

Table 3. TAB ground truth velocity model.

Layer	Depth (m)	Thickness (m)	V_S (m/s)	V_P (m/s)	ρ (kg/m^3)
1	0-1	1	192	438	1417
2	1-3	2	341	865	1573
3	3-5	2	671	1231	1699
4	5-8	3	998	1670	1841
5	8-11	3	1329	3238	2267
6	>11	-	1886	3863	2401

Table 4. MTC ground truth velocity model.

Layer	Depth (m)	Thickness (m)	V_S (m/s)	V_P (m/s)	ρ (kg/m^3)
1	0-1.5	1.5	200	443	1419
2	1.5-2.5	1	509	886	1581
3	2.5-3.5	1	673	1252	1706
4	3.5-5	1.5	849	1543	1801
5	5-8	3	1172	2000	1941
6	>8	-	1346	2580	2104

Table 5. Minimum and maximum frequencies and wavelength recovered from different source offsets.

			Rayleigh Wave				Love Wave			
			f_{min} (Hz)	f_{max} (Hz)	λ_{min} (m)	λ_{max} (m)	f_{min} (Hz)	f_{max} (Hz)	λ_{min} (m)	λ_{max} (m)
TAS	Source Offset	1*dx*	13.7	94.7	1.84	50.96	8.3	76.7	2.66	68.35
		3*dx*	14.2	99.6	1.71	46.33	8.8	82.0	2.56	67.77
		6*dx*	14.2	89.8	1.95	48.95	9.3	80.6	2.57	55.78
		12*dx*	13.2	58.1	3.70	58.59	9.8	78.6	2.63	59.46
		24*dx*	16.6	67.9	2.76	46.69	10.3	56.2	3.79	58.41
TAB	Source Offset	1*dx*	20.0	85.0	2.04	32.63	12.2	99.6	1.83	61.88
		3*dx*	13.7	85.9	2.00	49.43	13.2	99.6	2.01	59.28
		6*dx*	13.7	85.9	2.00	59.80	13.2	99.6	2.13	69.42
		12*dx*	15.1	85.4	2.05	58.74	15.1	97.7	2.21	61.11
		24*dx*	15.1	81.5	2.11	59.19	16.1	99.6	2.27	54.84
MTC	Source Offset	1*dx*	26.4	87.9	3.13	38.83	23.4	75.2	3.06	64.96
		3*dx*	28.3	92.3	2.23	33.82	25.4	82.0	1.72	48.19
		6*dx*	27.8	64.0	4.54	35.8	27.8	70.3	3.02	45.65
		12*dx*	28.3	92.8	2.84	39.89	26.9	97.7	2.40	57.88
		24*dx*	PQ*	PQ	PQ	PQ	28.3	78.1	2.83	42.86

* PQ = poor quality

Table 6. Minimum and maximum frequencies and wavelength recovered from different source types.

			Rayleigh Wave				Love Wave			
			f_{min} (Hz)	f_{max} (Hz)	λ_{min} (m)	λ_{max} (m)	f_{min} (Hz)	f_{max} (Hz)	λ_{min} (m)	λ_{max} (m)
TAS	Source Type	20-lb	14.2	94.7	42.93	1.84	-	-	-	-
		AWD-0	13.2	17.6	41.09	60.24	-	-	-	-
		Hor. Al.	-	-	-	-	8.8	78.6	2.71	67.28
		Hor. Wd.	-	-	-	-	8.3	82.0	2.56	68.73
		AWD-15	-	-	-	-	9.8	55.7	2.93	58.80
		AWD-30	-	-	-	-	9.8	50.8	3.77	54.03
		AWD-45	-	-	-	-	10.7	57.1	3.23	54.89
TAB	Source Type	20-lb	14.6	85.9	2.00	52.3	-	-	-	-
		AWD-0	14.2	85.4	2.04	58.64	-	-	-	-
		Hor. Al.	-	-	-	-	13.7	99.6	2.07	55.06
		Hor. Wd.	-	-	-	-	12.2	84.5	1.71	65.73
		AWD-15	-	-	-	-	13.2	99.6	2.04	63.07
		AWD-30	-	-	-	-	15.1	97.7	2.15	50.50
		AWD-45	-	-	-	-	14.2	99.6	2.08	62.66
MTC	Source Type	20-lb	27.8	84.0	2.94	36.51	-	-	-	-
		AWD-0	27.8	92.8	2.80	37.05	-	-	-	-
		Hor. Al.	-	-	-	-	23.4	72.3	2.81	67.44
		Hor. Wd.	-	-	-	-	23.9	82.0	1.72	57.20
		AWD-15	-	-	-	-	26.9	97.7	2.45	44.28
		AWD-30	-	-	-	-	25.4	96.7	2.34	60.12
		AWD-45	-	-	-	-	26.4	75.2	3.12	48.86

Table 7. Minimum and maximum frequencies and wavelength recovered from different source types.

			Rayleigh Wave				Love Wave			
			f_{min} (Hz)	f_{max} (Hz)	λ_{min} (m)	λ_{max} (m)	f_{min} (Hz)	f_{max} (Hz)	λ_{min} (m)	λ_{max} (m)
TAS	*dx*	1.5 m	13.2	22.9	20.91	56.23	8.3	60.5	3.13	69.55
		1.0 m	14.2	79.6	2.21	40.56	11.2	57.1	3.21	39.63
		0.5 m	21.5	99.6	1.71	21.86	14.2	82.0	2.56	22.1
TAB	*dx*	1.5 m	13.7	64.9	2.98	58.90	12.2	76.7	2.99	65.64
		1.0 m	16.1	85.9	2.01	37.44	17.1	99.6	2.15	36.08
		0.5 m	20.0	81.5	2.09	20.74	17.1	99.6	2.01	23.16
MTC	*dx*	1.5 m	28.3	80.1	4.34	36.93	23.4	67.4	3.96	64.96
		1.0 m	26.4	92.8	2.81	38.18	27.8	78.1	2.83	38.56
		0.5 m	35.2	92.3	2.2	21.2	32.2	97.7	2.40	20.53

7. REFERENCES

Abbiss, C. P., 1981, Shear wave measurements of the elasticity of the ground: Géotechnique, **31**, no. 1, 91–104

Anbazhagan, P., and Sitharam, T.G., 2010, Seismic site classification using boreholes and shear wave velocity: assessing the suitable method for shallow engineering rock region: Proceeding GeoFlorida 2010, 1059-1068.

ASTM International, 2017, ASTM D7400-17 Standard Test Methods for Downhole Seismic Testing: ASTM International, West Conshohocken, PA. doi: https://doi.org/10.1520/D7400-17

Behm, M., and Snieder, R., 2013, Love waves from local traffic noise interferometry: The leading Edge, **32**, no. 6, 628-632.

Bohlen, T., Kugler, S., Klein, G., and Theilen, F., 2004, 1.5D Inversion of lateral variation of Scholte-wave dispersion: Geophysics, **69**, 330–344.

Boxberger, T., Picozzi, M., and Parolai. S., 2011, Shallow geology characterization using Rayleigh and Love wave dispersion curves derived from seismic noise array measurements: Journal of Applied Geophysics, **75**, no. 2, 345-354.

Burke, W.R., and Schofield, N.B., 2008, The multi-channel analysis of surface waves (MASW) method as a tool for ground improvement certification: Proceeding SAGEEP 2008, 1041-1055.

Butler, D.K., 2005, Near-surface geophysics: Society of Exploration Geophysics (SEG), Tulsa, OK. 731 pp.

Carnevale, M., and Park, C.B., 2010, Wave energy sources for MASW: Proceedings of Symposium on the Application of Geophysics to Engineering and Environmental Problems (SAGEEP 2010), Keystone, CO.

Cox, B.R. and Teague, D.P., 2016, Layering ratios: a systematic approach to the inversion of surface wave data in the absence of a priori information: Geophysical Journal International, **207**(1), 422-438.

Crice, D., 2011. Near-surface, downhole shear-wave surveys: A primer: The Leading Edge, **30**, no. 2, 164-171.

Dal Moro, G., and Ferigo, F., 2011, Joint analysis of Rayleigh- and Love-wave dispersion: Issues, criteria and improvements: Journal of Applied Geophysics, **75**, no. 3, 573-589.

Dibiase, R., 2005, Seismic refraction analysis of sediment fill in Cyclone Graben, Needles District, Canyonlands national park: Proceedings of the 18th Keck Symposium, 11-15.

Eslick, R., Tsoflias, G., and Steeples, D., 2008, Field investigations of Love waves in near surface seismology: Geophysics, **73**, no. 3, p. G1–G6.

Fernandez, J.A., Rix, G.J., and Gowdy, S., 2008, Inversion Algorithm to Evaluate Velocity Profiles from Downhole Seismic Tests: Proceedings of Geotechnical Earthquake and Engineering and Soil Dynamics IV Congress 2008, 10 pp.

Forbriger, T., 2003a, Inversion of shallow-seismic wavefields: I. Wavefield transformation: Geophysical Journal International, **153**, 719–734.

Forbriger, T., 2003b, Inversion of shallow-seismic wavefields: II. Inferring subsurface properties from wavefield transforms: Geophysical Journal International, **153**, 735–752.

Foti, S., Hollender, F., Garofalo, F., Albarello, D., Asten, M., Bard, P., Comina, C., Cornou., Cox, B., Di Giulio, G., Forbriger., T., Hayashi., K., Lunedei., E., Martin., A., Mercerat., D., Ohrnberger., M., Poggi., V., Renalier., F., Sicilia., D., Socco., V., 2017, Guidelines for the good practice of surface wave analysis: a product of the InterPACIFIC project: Bull Earthquake Eng, doi: 10.1007/s10518-017-0206-7

Foti, S., Lai, C.G., Rix, G.J., and Strobbia, C., 2015, Surface wave methods for near-surface site characterization: CRC Press, 467 pp.

Green, R.A., Wood, C., Cox, B., Cubrinovski, M., Wotherspoon, L., Bradley, B., Algie, T., Allen, J., Bradshaw, A. and Rix, G., 2011, Use of DCP and SASW tests to evaluate liquefaction potential: Predictions vs. observations during the recent New Zealand earthquakes: Seismological Research Letters, **82**(6), 927-938.

Ha, I. S., Kim, N.R., and Lim, J.Y., 2013, Estimation of shear wave velocity of earth dam materials using artificial blasting test: Journal of the Korean Society of Civil Engineers, **33**, no. 2, 619-629.

Haines, S.S., 2007, A hammer-impact, aluminum, shear-wave seismic source Open-File Report 2007–1406: U.S. Department of Interior, U.S. Geological Survey, Reston, VA.

Heisey, J. S., Stokoe II, K. H., and Meyer, A. H., 1982, Moduli of Pavement Systems From Spectral Analysis of Surface Waves: Transportation Research Record, v. 852, Washington, D.C.

Herbst, R., Kapp, I., Krummel, H., and Luck, E., 1998, Seismic sources for shallow investigations: A field comparison from Northern Germany: Journal of Applied Geophysics, **38**, no. 4, 301-3017.

Ivanov J., Miller R.D., Lacombe P., Johnson C.D., and Lane J.W. Jr., 2006, Delineating a shallow fault zone and dipping bedrock strata using multichannel analysis of surface waves with a land streamer, Geophysics, **71**, no. 5, A39–A42.

Joh, S., Stokoe, K. H., Lee, I., Kang, T., Rosenbld, B., and Bay, J. A., 2006, Joint inversion for apparent phase velocities of Rayleigh and Love waves: Proceedings GeoCongress 2006, 1-6.

Jones, R., 1955, A vibration method for measuring the thickness of concrete road slabs in situ: Magazine of Concrete Research, **7**, no. 20, 97–102,

Jones, R., 1958, In-situ measurement of the dynamic properties of soil by vibration methods: Géotechnique, **8**, no. 1, 1–21.

Kanlı, A.I., Tildy, P., Pronay, Z., Pınar, A., and Hermann, L., 2006, VS30 mapping and soil classification for seismic site effect evaluation in Dinar region, SW Turkey: Geophysical Journal International, **165**, no. 1, 223-235.

Kim, D.S., Shin, M.K. and Park, H.C., 2001. Evaluation of density in layer compaction using SASW method. Soil Dynamics and Earthquake Engineering, **21**, no. 1, 39-46.

Konstantaki, L. A., Ghose, R., Draganov, D., Diaferia, G., and Heimovaara, T., 2015, Characterization of a heterogeneous landfill using seismic and electrical resistivity data: Geophysics, **80**, no. 1, EN13-EN25.

Lane, J. D., 2009, Geotechnical site characterization using multi-channel analysis of Rayleigh and Love waves, M.Sc. thesis, The University of Tennessee, USA.

Love, A.E., 1911, Some problems of geodynamics: Cambridge University Press.

Ludwig, W. J., Nafe, J. E.and Drake, C. L., 1970, Seismic refraction: *The Sea,* A. E. Maxwell, (Editor) Vol. 4, Wiley-Interscience, New York, 53–84.

Madhyannapu, R.S., Puppala, A.J., Nazarian, S. and Yuan, D., 2009, Quality assessment and quality control of deep soil mixing construction for stabilizing expansive subsoils: Journal of geotechnical and geoenvironmental engineering, **136**(1), 119-128.

Mahvelati, S., and Coe, J.T., 2017, Multichannel Analysis of Surface Waves (MASW) Using Both Rayleigh and Love Waves to Characterize Site Conditions: Proceedings of Geotechnical Frontiers 2017, Orlando, 647-656.

McMechan, G. A., and Yedlin, M. J., 1981, Analysis of dispersive waves by wave field transformation: Geophysics, **46**, 869-874.

Mi, B., Xia, J., Shen, C., and Wang, L., 2016, Dispersion energy analysis of Rayleigh and Love waves using finite-difference modeling: Proceedings 7th International Conference on Environmental and Engineering Geophysics & Summit Forum of Chinese Academy of Engineering on Engineering Science and Technology.

Miller, R.D., Pullan, S.E., Waldner, J.S., and Haeni, F.P., 1986, Field comparison of shallow seismic sources: Geophysics, **51**(11), 2067-2092.

Miller R.D., Xia J., Park C.B., and Ivanov J., 1999, Multichannel analysis of surface waves to map bedrock: Leading Edge, **18**, 1392–1396.

Milsom, J., and Eriksen, A., 2011, Field geophysics: Wiley, 282 pp.

Misiek, R., Liebig, A., Gyulai, A., Ormos, T., Dobroka, M., and Dresen, L., 1997, A joint inversion algorithm to process geoelectric and surface wave seismic data. Part II: applications: Geophysical Prospecting, **45**, no. 1, 65-85.

Motazedian, D., Hunter, J.A., Sivathayalan, S., and Khaheshi Banab, K., 2012, Railway train induced ground vibrations in a low V_S soil layer overlying a high V_S bedrock in eastern Canada: Soil Dynamics and Earthquake Engineering, **36**, 1-11.

Nazarian, S., K. H. Stokoe II, and W. R. Hudson, 1983, Use of spectral analysis of surface waves method for determination of moduli and thicknesses of pavement systems: Transportation Research Record: Journal of the Transportation Research Board, **930**, 38–45.

Nolan, J.J., Miller, R., Ivanov, I., and Peterie, S., 2013 Near-surface salt dissolution void identification using passive MASW: SEG Annual Meeting Expanded Abstracts, 2212-2217.

Obando, E.A., Park, C.B., Ryden, N., and Ulriksen, P., 2009, Roadside MASW surveys using a portable road bump, a case study in Managua, Nicaragua: Proceedings of Symposium on the Application of Geophysics to Engineering and Environmental Problems 2009, 626-635.

O'Neill, A., 2003, Full-waveform reflectivity for modelling, inversion and appraisal of seismic surface wave dispersion in shallow site investigations: Ph.D. thesis (Unpublished), The University of Western Australia, School of Earth and Geographical Sciences.

O'Neill, A., 2004, Full waveform reflectivity for inversion of surface wave dispersion in shallow site investigations: Proceedings of Symposium on the Application of Geophysics to Engineering and Environmental Problems 2004, 1565-1576.

Park, C.B., Miller, R.D., and Xia, J., 1998, Imaging dispersion curves of surface waves on multi-channel record: SEG Technical Program Expanded Abstracts 1998, 1377-1380.

Park, C.B., and Carnevale, M., 2010, Optimum MASW survey-revisit after a decade of use: GeoFlorida 2010, 1303-1312.

Park, C.B., and Carnevale, M., 2014, Multichannel analysis of surface waves (MASW): Symposium on the Application of Geophysics to Engineering and Environmental Problems (SAGEEP 2014), Boston, March 16-20, Short Course Notes.

Park, C. B., and R. D. Miller, 2008, Roadside passive multichannel analysis of surface waves (MASW): Journal of Environmental and Engineering Geophysics, **13**, 1-11.

Park, C.B., Miller, R.D., and Miura, H., 2002, Optimum field parameters of an MASW survey: Japanese Society of Exploration Geophysics (SEG-J) Extended Abstracts, Tokyo, Japan.

Park, C.B., Miller, R.D., and Xia, J., 1999, Multichannel analysis of wurface waves: Geophysics, **64**, no. 3, 800-808.

Renalier, F., Bièvre, G., Jongmans, D., Campillo, M., and Bard, P.-Y., 2010, Clayey landslide investigations using active and passive V_S measurements: Chapter 24 in Advances in Near-surface Seismology and Ground-penetrating Radar, Geophysical Developments Series No. 15, 397-414

Safani, J., O'Neill, A. O., Matsuoka, T., and Sanada. Y., 2005, Applications of Love wave dispersion for improved shear-wave velocity imaging: Journal of Environmental and Engineering Geophysics, **10**, no. 2, 135-150.

Song, Y., Castagna, J. P., Black, R. A., Knapp, R. W., 1989, Sensitivity of near-surface shear wave velocity determination from Rayleigh and Love waves: 59th Annual International Meeting, SEG, Expanded Abstracts, 509–512.

Stokoe II, K.H., and Santamarina, J.C., 2000, Seismic-wave-based testing in geotechnical engineering: International conference on geotechnical and geological engineering; GeoEng 2000, 1490-1536.

Stokoe II, K.H., Wright, G. W., Bay, J. A., and Roesset, J. M., 1994, Characterization of geotechnical sites by SASW method: Geophysical characterization of sites, R. D. Woods, Ed. A.A. Balkema, Rotterdam, 15-25.

Tokimatsu, K., 1995, Geotechnical site characterization using surface waves: Proceedings of the 1st International Conference on Earthquake Geotechnical Engineering, Balkema, Rotterdam, 1333-1368.

Van der Poel, C., 1951, Dynamic testing of road constructions: Journal of Applied Chemistry, **1**, 281–290.

Waddell, P.J., Moyle, R.A., and Whiteley, R.J., 2010, Geotechnical verification of impact compaction: Proceedings 7th Int'l Conf. on computer simulation in risk analysis and hazard mitigation., WIT Press, Algarve.

Xia, J., 2014, Estimation of near-surface shear-wave velocities and quality factors using multichannel analysis of surface-wave methods: Journal of Applied Geophysics, **103**, 140-151.

Xia, J., Miller, R.D., Cakir, R., Luo, Y., Xu, Y., Zeng, C., 2010, Revisiting SH-wave data using Love-wave analysis: Proceedings SAGEEP 2010, 569-580.

Xia, J., Miller, R.D., and Park, C.B., 1999, Estimation of near-surface shear-wave velocity by inversion of Rayleigh waves: Geophysics, **64**, no. 3, 691–700.

Xia J., Chen C., Li P.H., and Lewis M.J., 2004, Delineation of a collapse feature in a noisy environment using a multichannel surface wave technique: Geotechnique, **54**, no. 1, 17–27.

Xia J., Nyquist J.E., Xu Y., Roth M.J.S., and Miller R.D., 2007, Feasibility of detecting near-surface feature with Rayleigh-wave diffraction: Journal of Applied Geophysics, **62**, no. 3, 244–253.

Xia, J., Xu, Y., Luo, Y., Miller, R.D., Cakir, R., and Zeng, C., 2012, Advantages of using Multichannel analysis of Love waves (MALW) to estimate near-surface shear-wave velocity: Surveys in Geophysics, **33**, no. 5, 841–860.

Yilmaz, O., Eser, M., and Berilgen, M., 2009, Applications of engineering seismology for site characterization: Journal of Earth Science, **20**, no. 3, 546–554.

Yin, X., Xia, J., Shen, C., and Xu, H., 2014, Comparative analysis on penetrating depth of high-frequency Rayleigh and Love waves: Journal of Applied Geophysics, **111**, 86-94.

Yong, A., Martin, A., Stokoe, K., and Diehl, J., 2013, ARRA-funded VS30 measurements using multi-technique approach at strong-motion stations in California and central-eastern United States: U.S. Geological Survey Open-File Report 2013–1102, 60 p. and data files, http://pubs.usgs.gov/of/2013/1102/.

Yoon, S., 2005, Array-based measurements of surface wave dispersion and attenuation using frequency-wavenumber analysis, Ph.D. dissertation, Georgia Institute of Technology, Atlanta, Ga.

Yoon, S., Rix, G.J., 2009, Near-field effects on array-based surface wave methods with active sources: Journal of Geotechnical and Geoenvironmental Engineering, 135, no. 3., 399-406.

Yordkayhun, S., Ivanova, A., Giese, R., Juhlin, C., and Cosma, C., 2009, Comparison of surface seismic sources at the CO2SINK site, Ketzin, Germany: Geophysical Prospecting, **57**, no. 1, 125-139.

Zeng, C., Xia, J., Liang, Q., and Chen, C., 2007, Comparative analysis on sensitivities of Love and Rayleigh waves: Proceedings of SEG/San Antonio 2007 Annual Meeting, 1138-1141.

Zeng, C., Xia, J., Miller, R.D., Tsoflias, G.P., and Wang, Z., 2012, Numerical investigation of MASW applications in presence of surface topography: Journal of Applied Geophysics, **84,** 52-60.

8. APPENDICES

The complete collection of dispersion images for all testing can be found at the following website: https://sites.google.com/a/temple.edu/joseph-coe/research/usgs-g15ap00024